EVALUATING BOREABILITY OF METAMORPHIC ROCKS: INTEGRATING TEXTURE COEFFICIENT, ROCK ABRASIVITY, AND OPERATIONAL PARAMETERS FOR ENHANCED TBM PERFORMANCE PREDICTION

by

GLEB SMIRNOV

THESIS SUPERVISOR
SAFFET YAGIZ

Thesis submitted to the School of Mining and Geosciences of Nazarbayev University in Partial Fulfillment of the Requirements for the Degree of

Master of Science in Mining Engineering

Nazarbayev University

3rd of May 2025

ORIGINALITY STATEMENT

I, Gleb Smirnov, hereby declare that this submission is my own work and to the best of my knowledge it contains no materials previously published or written by another person, or substantial proportions of material which have been accepted for the award of any other degree or diploma at Nazarbayev University or any other educational institution, except where due acknowledgement is made in the thesis.

Any contribution made to the research by others, with whom I have worked at NU or elsewhere, is explicitly acknowledged in the thesis.

I also declare that the intellectual content of this thesis is the product of my own work, except to the extent that assistance from others in the project's design and conception or in style, presentation, and linguistic expression is acknowledged.

Signed on 3.05.2025

_____

ABSTRACT

The efficiency and cost-effectiveness of mechanized tunneling in hard rock conditions are closely tied to the geological characteristics of the rock mass, particularly its texture and mechanical properties. This study investigates the potential of assessing rock boreability using the Texture Coefficient (TC), which quantifies rock texture based on grain shape, orientation, and interlocking. By examining the relationship between TC, other physical rock properties, and Tunnel Boring Machine (TBM) performance, this research aims to improve the prediction of Rate of Penetration (ROP) and support effective tunneling strategies.

The methodology is based on the analysis of rock samples collected from the Queens Water Tunnel excavation project in New York City, 1996-1999. Thin sections of the rock samples were examined using image analysis software (ImageJ), following the TC identification procedure outlined by Howarth and Rowlands (1987). Additionally, mechanical and physical properties, including Uniaxial Compressive Strength (UCS), Brazilian Tensile Strength (BTS), Cerchar Abrasivity Index (CAI), and others, were obtained from previously performed laboratory tests. TBM performance parameters such as penetration rate, thrust, torque, and power were gathered from field data recorded during excavation.

The linear and nonlinear regression models were developed to estimate the TBM penetration rate using TC, UCS, CAI, Cutterhead Power (CP), and Alpha Angle as input variables. The analysis indicated that CP and CAI strongly influenced ROP prediction, while the contribution of other variables was less significant. The most optimal models achieved a considerable degree of fit with R^2 values between 0.82 and 0.85, indicating a strong correlation between the input parameters and actual TBM performance.

The results show that the application of TC for TBM performance prediction models is limited in its current form. Despite the overall high predictive power of the presented models, the TC plays an insignificant role if included in the model, occasionally increasing the prediction error. Future work may explore the potential modifications of TC depending on the rock type and the automation of the TC calculation process, improving its practicality for research and engineering applications.

ACKNOWLEDGMENT

First and foremost, I would like to express my gratitude to my supervisor, Professor Saffet Yagiz, for his invaluable guidance, support, and encouragement throughout the preparation of this thesis. His expertise as both a scientist and a professional in the field of rock mechanics and tunnel engineering has been crucial in keeping the direction and quality of this research. I am especially thankful for the dataset he provided, which served as the foundation for this work.

I would also like to thank Professors Amoussou Coffi Adoko, Roohollah Shirani Faradonbeh, and Nasser Madani for their professional advice and constructive feedback on my thesis, which greatly contributed to the refinement and improvement of this work.

Finally, I am thankful to Toluwase Daniel Olaiya, an MSc student in the same program, for his support and assistance during the statistical analysis phase. His willingness to share his time and knowledge significantly contributed to the successful completion of the analytical component of this study.

This research was funded by the School of Mining and Geosciences, Nazarbayev University, under the Faculty Development Grant Program (Grant No. 201223FD8837) for which I am grateful.

TABLE OF CONTENTS

LIST OF FIGURES

LIST OF TABLES

LIST OF ABBREVIATIONS

ANOVA	Analysis of Variance
AF	Angle Factor
AR	Aspect Ratio
BI	Brittleness Index (kN/mm)
BTS	Brazilian Tensile Strength (MPa)
CAI	Cerchar Abrasivity Index
CP	Cutterhead Power (kW)
CSM	Colorado School of Mines
FF	Form Factor
IQR	Interquartile Range
NTNU	Norwegian University of Science and Technology
ROP	Rate of Penetration (m/hr)
RPM	Rotations per Minute
SE	Specific Energy (MJ/m^3)
TBM	Tunnel Boring Machine
TC	Texture Coefficient
UCS	Uniaxial Compressive Strength (MPa)
VIF	Variance Inflation Factor
α	Alpha Angle (°)

CHAPTER 1 – INTRODUCTION

1.1. Background

Mechanized excavation using Tunnel Boring Machines (TBMs) has revolutionized underground construction, allowing for efficient excavation in various geological formations. Over the past few decades, TBMs have been widely adopted in civil and mining engineering projects due to their ability to enhance the safety of human operators, reduce environmental impact, and improve tunneling efficiency (Pandey et al., 2020). However, in certain geological conditions, predicting TBM performance remains a significant challenge due to the variability in rock properties, which influence penetration rates, tool wear, and overall excavation efficiency.

Traditional predictive models, such as those developed by the Colorado School of Mines (CSM) and the Norwegian University of Science and Technology (NTNU), primarily rely on geomechanical parameters like Uniaxial Compressive Strength (UCS) and indices of rock mass quality such as Drilling Rate Index, as well as machine parameters including Rotations per Minute (RPM), Penetration Rate, and cutter characteristics. These models have proven effective in homogeneous rock formations but can be less reliable in geologically complex terrains where lithological variability is high. For example, studies have shown that TBM performance in metamorphic formations with high mineral heterogeneity, especially in those rich in abrasive minerals like quartz and garnet, characteristic of the metamorphic rocks, can significantly differ from predictions based on UCS alone, with actual penetration rates being up to 35% lower than expected (Merguerian & Ozdemir, 2003).

Recent studies have highlighted the importance of rock texture in influencing excavation performance. The Texture Coefficient (TC), initially introduced by Howarth & Rowlands (1987), quantifies rock texture based on matrix amount and grain shape and orientation, offering a more geologically oriented parameter for assessing boreability. The TC provides a measure of how different mineralogical components interact at the grain level, which directly affects the mechanical fragmentation of the rock. Research has demonstrated that TC values correlate with TBM performance metrics such as Rate of Penetration (ROP). For instance, Suorineni et al. (2009) found that the correlative relationships between TC and TBM Penetration Rate were much stronger than that of the ratio of the rock's compressive and tensile strengths, reaching R^2 values above 0.99 for sedimentary rocks. This evidence indicates that lithological factors beyond rock strength

significantly influence TBM efficiency. Similarly, Tumac et al. (2018) demonstrated that integrating TC into the mechanized excavation performance models resulted in an improvement in cutting rate predictions for projects in metamorphic formations. These findings highlight the need to refine existing boreability models by incorporating texture-based parameters.

1.2. Problem Definition

The effectiveness of TBM excavation is significantly influenced by rock texture, yet traditional geomechanical models often overlook this aspect. The standard UCS-based models may not provide accurate performance predictions in metamorphic rock formations, where textural characteristics like matrix amount, grain shape, and interlocking, which may significantly influence the excavation efficiency, vary considerably (Ribacchi & Lembo Fazio, 2005). Thus, there is a need for an improved predictive framework that incorporates texture-based parameters for complex geological terrains.

This research aims to address this gap by evaluating boreability in metamorphic formations through the integration of the Texture Coefficient and physical parameters of the rocks. By analyzing the relationship between TC, rock mechanical and physical properties, and TBM performance, the study seeks to enhance boreability assessments and establish a model for excavation rate prediction.

1.3. Objectives of the Thesis

The primary objectives of this study are:

1. To quantify the Texture Coefficient from thin section images of metamorphic rocks using digital image analysis techniques.
2. To evaluate the influence of TC and selected physical and mechanical rock properties on the TBM penetration rate.
3. To develop a predictive model for estimating the Rate of Penetration by integrating TC, rock properties, and TBM operational parameters.

1.4. Methodology

This study follows a structured approach, beginning with identifying the Texture Coefficients for the available rock sample thin sections using image analysis software. This process involves characterizing grain morphology, relative orientation, and the distribution of mineral components within the rock samples. The processing of thin section photomicrographs allows for extracting the grain geometrical parameters, used in the calculation of TC, which serves as the first input into the comprehensive dataset for statistical analysis.

The remaining portion of the dataset is then prepared and consists of previously collected and tested rock property data, including UCS, Brazilian Tensile Strength (BTS), density, Cerchar Abrasivity Index (CAI) and Mohs Hardness, as well as the TBM field performance data, including ROP, thrust, power, and torque (Yagiz, 2002). Before analysis, the dataset undergoes review and unit conversions to ensure consistency and comparability of parameters across different sources.

The statistical analysis is performed using regression techniques in SPSS software. This step involves correlating ROP with TC, mechanical and physical rock properties, as well as other TBM operational parameters to evaluate the predictive power of texture-based models. Multiple regression models, including linear and non-linear approaches, are tested to determine the most accurate representation of the relationship between rock texture and boreability.

1.5. Thesis Outline

Chapter 1 provides an introduction, outlining the research background, problem definition, objectives, and methodology.

Chapter 2 presents a comprehensive literature review of rock texture analysis, boreability models, and the significance of TC in mechanized excavation, as well as the geological setting and rock characteristics of the study area, with emphasis on the metamorphic formations encountered in the TBM project.

Chapter 3 explains the thesis methodology, particularly the experimental procedures for petrographic and statistical analysis, including TC computation and database preparation.

Chapter 4 presents the results of the regression analysis, highlighting correlations between TC, rock properties, and TBM performance metrics, and provides the obtained predictive model equations.

Chapter 5 discusses the implications of the findings, selecting the most optimal models from the ones obtained during the multivariable linear and non-linear regression analyses.

Chapter 6 concludes the study, summarizing key findings and offering recommendations for future research on texture-based boreability assessment in tunneling projects.

CHAPTER 2 – LITERATURE REVIEW

2.1. Introduction

Rock texture plays a crucial role in determining the mechanical behavior of rock masses, influencing their strength and boreability. Various studies have investigated the correlation between rock texture, quantified through the Texture Coefficient, and geomechanical properties such as UCS, tensile strength, and drillability (Howarth & Rowlands, 1987; Azzoni et al., 1996). The ability to predict the mechanical response of rock materials based on their textural properties has significant implications for excavation and tunneling projects, particularly those utilizing Tunnel Boring Machines.

One of the primary reasons TC has gained attention in excavation performance assessment is its ability to provide a more detailed representation of rock microstructure compared to conventional geomechanical indices. Traditional rock classification systems, such as the Rock Mass Rating and Q-system, primarily focus on macroscopic characteristics, including joint spacing, roughness, and weathering, usually ignoring the influence of grain interlocking and mineral distribution at the microscopic scale. Studies such as Ribacchi & Lembo Fazio (2005) and Hassanpour et al. (2011) highlight that avoiding consideration of textural characteristics can lead to significant misinterpretations of TBM performance predictions, particularly in heterogeneous rock masses. Ignoring texture-related features such as grain size, grain boundary interlocking, matrix content, and mineral alignment can result in inaccurate estimates of penetration rate and tool wear. In metamorphic and other heterogeneous rocks, similar strength values (e.g., UCS) may correspond to drastically different excavation behaviors because texture controls fracture propagation, chipping mechanisms, and cutter-rock interaction. Without accounting for textural variability, predictive models may either underestimate resistance in highly interlocked rocks or overestimate performance in weaker, foliated zones, ultimately leading to less accurate predictions, project delays, or increased maintenance costs during tunneling operations.

2.2. The Texture Coefficient Concept

Howarth and Rowlands (1987) introduced the TC as a quantitative measure of rock texture based on grain shape, orientation, interlocking, and packing density. Their study demonstrated a strong correlation between TC and both drillability and strength properties. The original

formulation of TC relied on image analysis of thin sections to obtain geometric characteristics of grains and matrix, therefore offering an objective measure of rock fabric properties.

Subsequent research by Azzoni et al. (1996) confirmed these relationships, highlighting that igneous rocks typically exhibit higher TC values than sedimentary and metamorphic rocks. The study also established that higher TC values correlate with increased resistance to fragmentation and lower rates of penetration in excavation projects. Their results supported the argument that TC is a key indicator of rock boreability and should be incorporated into predictive models for excavation performance.

Further advancements in TC applications were made by Ozturk et al. (2014), who developed regression models linking TC to UCS, reporting R^2 values above 0.90 for specific lithologies, particularly within the group of sedimentary rocks (Figure 2.1). Studies such as those by Tugrul & Zarif (1999) and Ozturk & Nasuf (2013) have also examined the influence of textural properties on rock strength and classification, demonstrating that TC can be effectively used for strength estimation in various rock types.

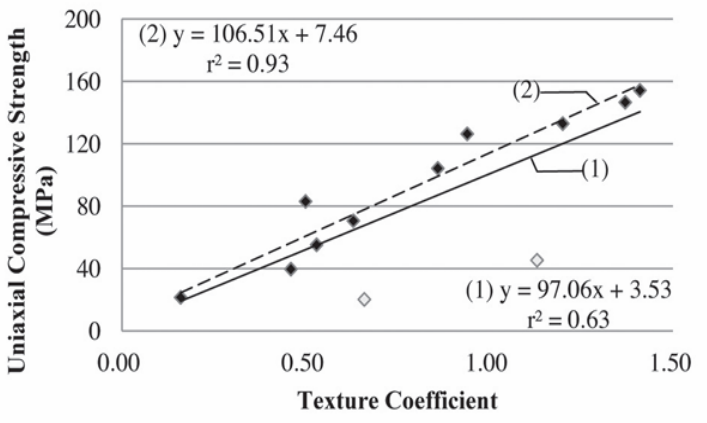

Figure 2.1. Correlation between UCS and TC for sandstone, siltstone, marl, and shale (Line 2; Ozturk et al., 2014)

Recent studies, such as those by Çomaklı and Atıcı (2022), have explored artificial intelligence techniques for improving TC-based predictive models, demonstrating enhanced accuracy using neural networks and regression approaches. The study links rock density, Schmidt hardness, and Ultrasonic P-wave velocity together with TC for a versatile estimation model. The integration of machine learning algorithms has enabled more sophisticated analysis of texture parameters, providing refined predictions of rock strength and boreability.

2.3. TC and Its Relationship with Geomechanical Properties

The TC is closely linked to various geomechanical parameters, including UCS, BTS, CAI, and porosity. Studies by Howarth & Rowlands (1987) and Azzoni et al. (1996) have shown that TC correlates strongly with UCS, with higher TC values generally corresponding to increased compressive strength. Bayram et al. (2011) and Atici & Çomaklı (2019) further established correlations between TC and mechanical properties such as elasticity modulus and density, enhancing its role as a prospective predictor of rock behavior.

Bayram et al. (2011) reported that TC values in granitic rocks exhibited a strong correlation ($R^2 = 0.85$) with UCS, while elasticity modulus showed an R^2 value of 0.81. Additionally, Ozturk et al. (2014) found that for limestone samples, TC values were inversely related to drillability, with a reduction in penetration rates of up to 25% in high-TC rocks. The study by Tumac et al. (2017) on sedimentary and metamorphic rocks found that TC values above 2.0 corresponded to a significant increase in specific cutting energy, indicating a direct relationship between texture characteristics and excavation difficulty (Figure 2.2).

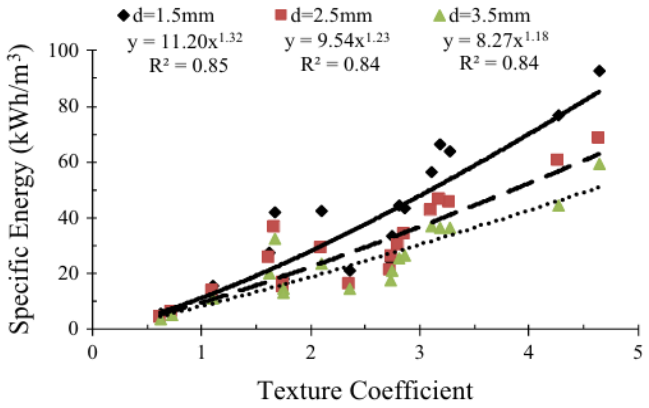

Figure 2.2. Relationship between TC and SE (Tumac et al., 2017)

Additionally, Ozturk et al. (2014) identified that TC exhibits a strong inverse relationship with rock drillability, particularly at higher TC, where the efficiency of percussive and rotary drilling decreases. This relationship is especially relevant for TBM excavation, where high TC values indicate greater resistance to mechanical penetration. Moreover, TC has been found to influence tool consumption rates, with highly interlocked grain structures contributing to increased tool wear, as noted by Tumac et al. (2017) through the correlations with Specific Energy (SE)

consumption for the chisel tools. Studies by Tiryaki and Dikmen (2005) and Tumac et al. (2018) have further analyzed the impact of textural properties on cutting energy and tool wear in excavation processes.

2.4. Influence of TC on Boreability and TBM Performance

Several case studies, including those presented by Bilgin et al. (2016), have investigated TBM performance in difficult ground conditions. These studies highlight the necessity of incorporating TC into excavation models to better predict penetration rates and cutter wear, particularly in high-strength rock formations. Rocks with high TC values often require increased cutter thrust and torque, leading to higher energy consumption and reduced advance rates. Conversely, rocks with lower TC values tend to be more susceptible to mechanical fragmentation, facilitating higher penetration rates.

Bilgin et al. (2016) provided insights into excavation challenges caused by high-strength and highly interlocked rock masses. Their research demonstrated that traditional UCS-based models often underestimate the impact of texture-related factors, leading to discrepancies in performance predictions. Studies by Ribacchi & Lembo Fazio (2005) and Delisio et al. (2012) have shown that joint spacing and blocky rock conditions paired with high rock texture cohesion significantly affect TBM performance, indicating that textural parameters play a critical role in boreability assessments.

Furthermore, recent advancements in TBM performance modeling, such as the Ylvie model introduced by Schlicke et al. (2024), integrate machine learning approaches to refine penetration rate predictions by analyzing operational TBM data, resulting in more accurate performance prediction compared to the conventional methods like the CSM and Gehring models (Figure 2.3). This method demonstrates the potential for combining traditional geotechnical assessments with modern computational techniques for improved excavation planning. Similarly, integrating TC with existing TBM performance models could significantly enhance boreability assessments. A potential direction for future research would be incorporating TC with real-time TBM operational data, which would allow for dynamic adjustments to excavation parameters based on encountered rock conditions.

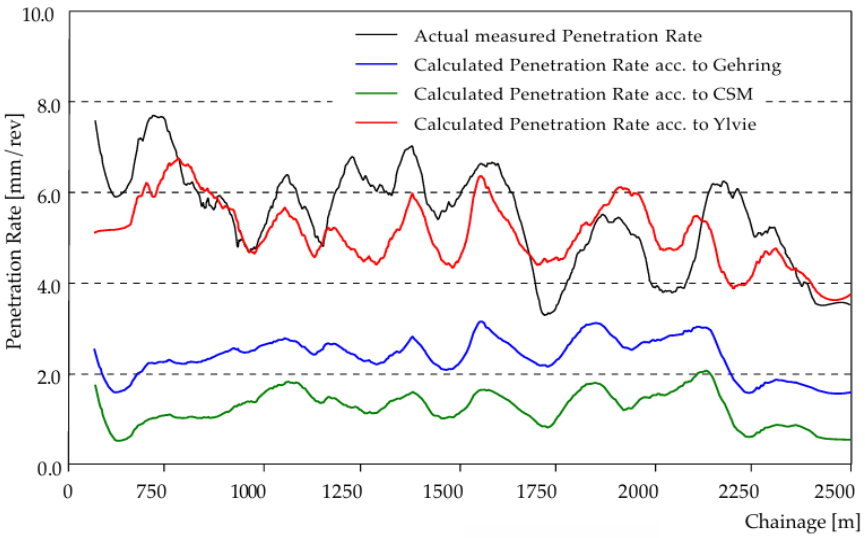

Figure 2.3. Comparison of penetration rate calculated using the CSM model, Gehring model, and the Ylvie model (Schlicke et al., 2024)

2.5. Advances in TC Measurement Techniques

Traditionally, TC has been measured through manual or semi-automated image analysis of thin sections using petrographic microscopes. This approach involves identifying individual grains, quantifying their shapes, sizes, and orientation patterns, and assigning numerical values to these characteristics. However, the manual nature of this process introduces variability due to subjective interpretation, leading to inconsistencies in measurements.

Recent technological advancements have led to the development of automated image-processing techniques using high-resolution digital microscopy. Software tools such as ImageJ, MATLAB, or AutoCAD-based algorithms (Figure 2.4) and deep learning models have been employed to extract textural parameters with greater precision (Ozturk et al., 2014; Tumac et al., 2017). Machine learning algorithms, such as convolutional neural networks, have been applied to automate grain boundary detection and texture quantification, significantly reducing processing time and human error (Çomaklı & Atıcı, 2022). These automated methods enable large-scale analysis of the rock thin sections with higher accuracy, making TC measurements more reliable and reproducible. However, it is necessary to note that such approaches at the moment are only applicable to relatively simple textures and grain characters, common for sedimentary rocks like sandstones and limestones, while in the cases of more complex textures, manual TC identification remains more applicable and accurate.

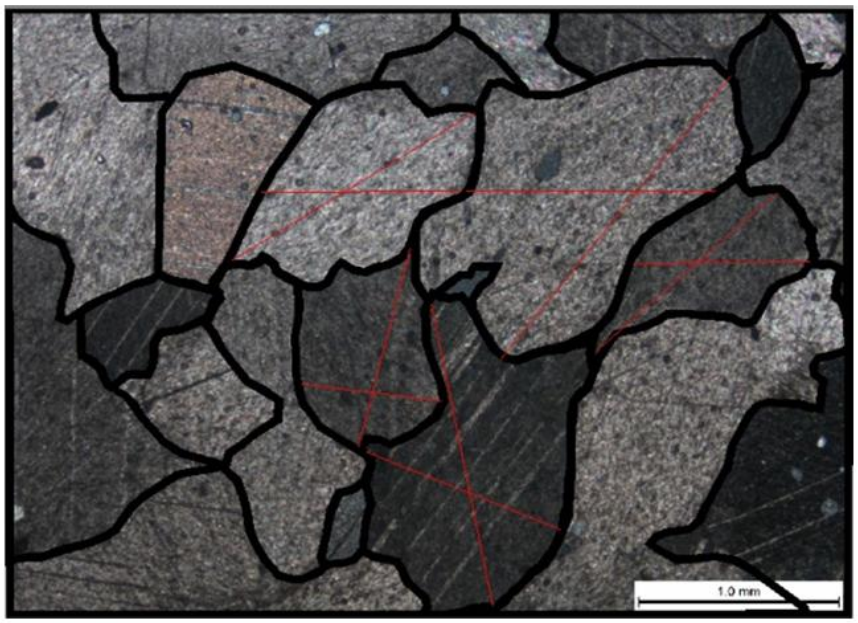

Figure 2.4. The view of a rock thin section with grain boundaries highlighted in the AutoCAD program (Tumac et al., 2017)

As seen from the literature review, the TC concept holds significant potential for TBM performance prediction and has already proved to be associated with various mechanical and operational parameters. It will be, thus, applied to the case study of the TBM project to uncover the details of interrelations between TC, geomechanical and rock mass properties, and machine performance metrics.

2.6. Case Study

The Queens Water Tunnel is a segment of New York City Water Tunnel No. 3 (Stage Two) that represents one of the largest infrastructure projects in the city's history (Table 2.1). With a final diameter of 7.7 m, a total excavated length of 7.6 km, and a maximum depth of 214 m below the ground surface, the tunnel traverses a geologically complex sequence of metamorphic bedrock (Merguerian, 1999). Construction commenced in 1996 using a Robbins TBM and concluded in 1999, exceeding the projected timeline due to operational delays. Field data revealed a significant divergence between predicted and achieved performance metrics: the actual average ROP reached only 1.8 m/hr, while the initial forecast was 2.75 m/hr (Merguerian & Ozdemir, 2003). This drop in efficiency prompted a post-construction investigation to identify the influencing factors, with particular emphasis on the interplay between TBM operational parameters and the unique lithological challenges posed by the host rock.

Table 2.1. Queens Water Tunnel TBM project information (Yagiz, 2002)

Total Length	7620	m	Cutter Diameter	482.6	mm
Total Diameter	7.7	m	Cutter Tip Width	19.05	mm
TBM Manufacturer	Robbins		Maximum Cutter Load	311.4	kN
TBM Type	Open Beam		Total Installed Thrust	15569	kN
No. of Cutters	50		Total Installed Power	3148	kW

2.7. Regional Geology

New York City is situated at the southern edge of the Manhattan Prong, a northeast-trending belt of metamorphic and igneous rocks belonging to the New England Appalachians (Figure 2.5). The project area is dominated by high-grade metamorphic rocks, including the Fordham Gneiss, Hartland Formation, and younger intrusive bodies (Merguerian, 1999). These formations have undergone multiple episodes of deformation and metamorphism, significantly influencing their textural and mechanical properties

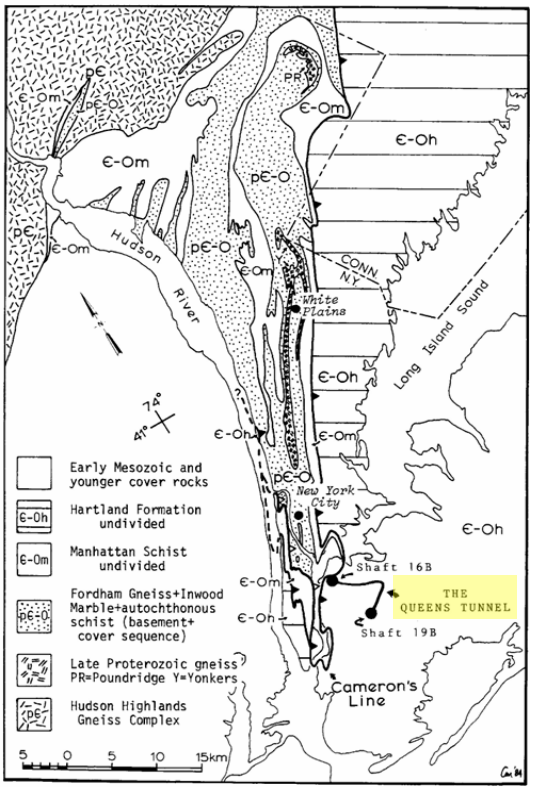

Figure 2.5. Simplified geological map of the Manhattan Prong belt (Merguerian, 1999)

The Fordham Gneiss Formation, dated approximately 1.0 Ga, consists primarily of granoblastic orthogneisses that underwent Grenvillian granulite facies metamorphism. The Hartland Formation, of the Cambrian-Ordovician age, is composed of aluminous metasedimentary rocks and metavolcanic sequences. The region has been affected by the Taconian, Acadian, and Alleghenian orogenies, which have further deformed and recrystallized the rock masses, producing complex structural features that impact TBM performance (Phillipson, 1998).

The lithological units encountered in the Queens Tunnel excavation include high-grade metamorphic rocks with a dominant presence of orthogneisses and, to a lesser extent, amphibolites. The rock mass consists of (Merguerian & Ozdemir, 2003; Figure 2.6):

- **Mafic- to Meso-Gneiss/Schist**: The predominant lithology in the tunnel area, composed of highly foliated, medium- to coarse-grained gneisses with alternating layers of feldspar-rich and biotite-rich bands. Elevated concentrations of garnet (up to 50%) are noted in this rock type. This lithology exhibits strong anisotropy, significantly affecting TBM cutting efficiency.
- **Granitic Gneiss**: Characterized by a granoblastic texture with a mineralogical composition composed of quartz, feldspar, and minor biotite, contributing to relatively high UCS values and moderate abrasivity.
- **Amphibolite**: Fine- to medium-grained amphibole-rich rock, occurring as interlayers within the gneisses. The strong foliation influences TBM penetration rates due to variations in cutting resistance.
- **Pegmatite**: Coarse-grained, feldspar-rich bodies with occasional quartz and mica. These igneous rocks create localized areas of high UCS but are generally less abrasive compared to gneisses.
- **Rhyodacite**: Hypabyssal intrusive dikes that introduce structural complexity, particularly along faulted zones.
- **Mafic Dikes**: Fine-grained, dark-colored intrusive bodies with high density and strength, potentially increasing disc cutter wear.

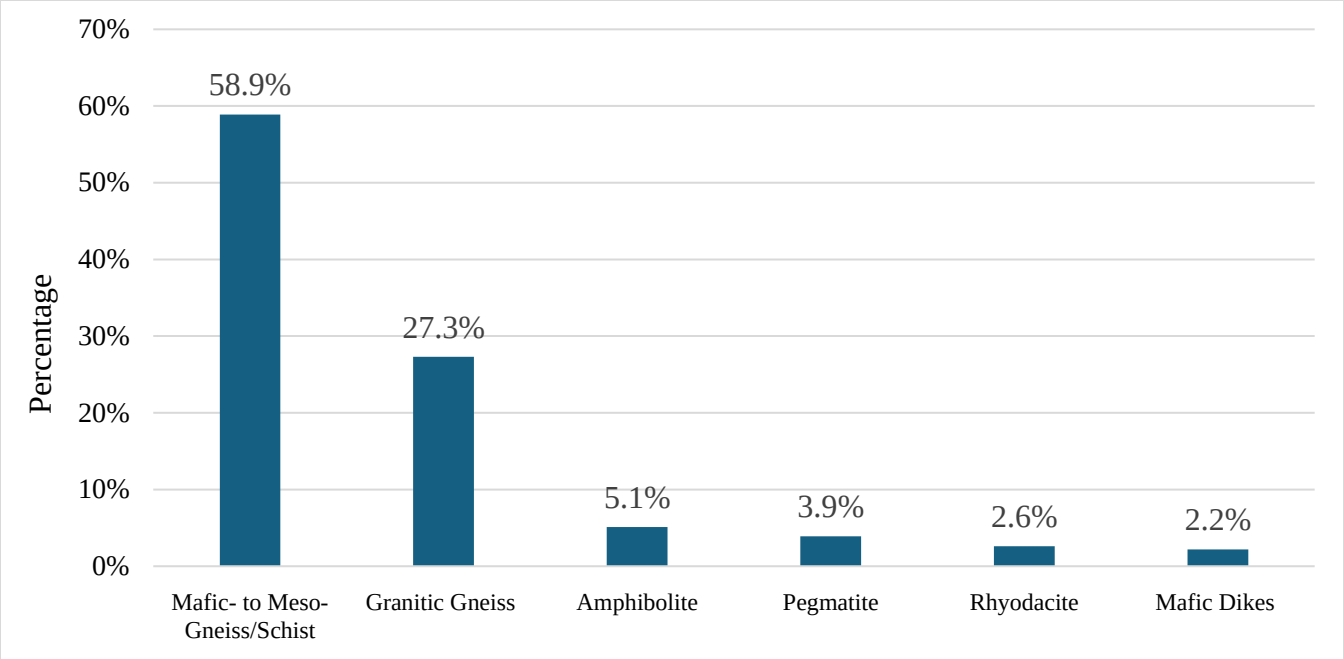

Figure 2.6. Lithological distribution of the Queens Tunnel Complex (after Yagiz, 2002)

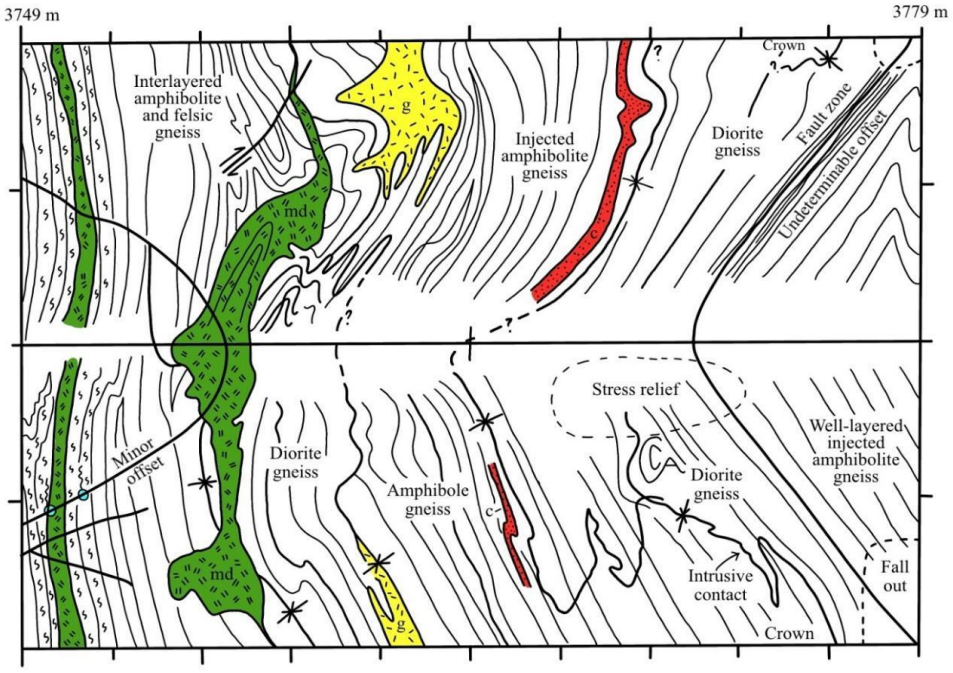

Figure 2.7. Schematic geologic map of the tunnel section from 3749 m to 3779 m (after Brock et al., 2000)

Figure 2.7 provides an example of the distribution of geological formations across the tunnel section. The majority of lithology is represented by gneisses (white); the rest include mafic dykes (md), pegmatitic granites (g), and garnet concentration (c) zones. Note the direction of the rock foliation compared to that of the tunnel direction, which further influences the mechanical fragmentation of the rock mass.

The Queens Tunnel is characterized by a complex structural history, with multiple deformation phases creating a diverse set of brittle and ductile geological structures. These include:

- **Ductile shear zones**: Associated with Proterozoic deformation events, producing mylonitic fabrics and imbricated rock masses (Merguerian, 2001).
- **Brittle faults**: Five generations of brittle faults have been identified, with dominant sets trending NNE and NW. These faults, outlined by zones of fault breccia and gouge, significantly impact TBM performance by inducing blocky ground and stress relief regions (Figure 2.8).
- **Folding**: Complex folding is observed, with isoclinal folds controlling lithological distribution and influencing the orientation of rock mass discontinuities.

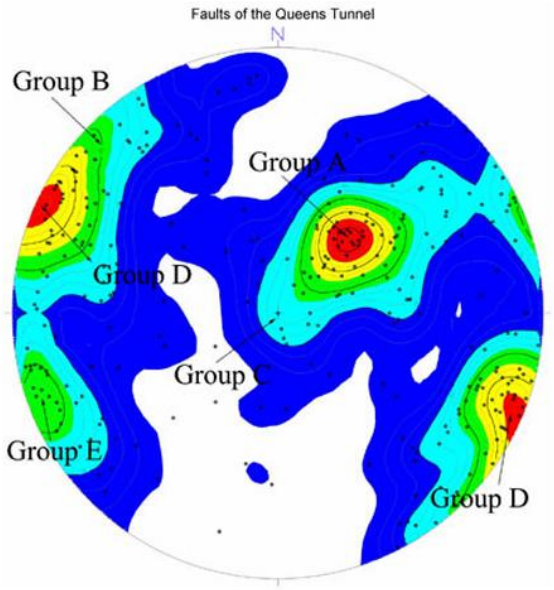

Figure 2.8. Stereonet plot of brittle fault orientations (Merguerian, 2001)

2.8. Rock Mass Properties and TBM Performance Implications

The geological characteristics of the Queens Tunnel rock mass directly influenced TBM performance, particularly penetration rates and tool wear. According to the available laboratory test results for the entire tunnel length, the rock UCS values ranged from 65 MPa to 273 MPa (Figure 2.9, a), corresponding to high to very high rock strength according to the International Society for Rock Mechanics standards. The Cerchar Abrasivity Index ranged between 2.9 and 5.3, indicating highly abrasive conditions, particularly in quartz-rich and garnet-bearing lithologies (Figure 2.9, b). The figures below are representative of the whole excavation; however, only a portion of the data could be analyzed by this research due to the limited number of prepared thin sections. The fracture spacing varies significantly, being as high as 15 m and above in some sections of the tunnel, but also reaching less than 0.1 m in fault shearing zones, inevitably affecting the excavation operation.

The TBM excavation was complicated by several factors. Blocky ground conditions, induced by brittle faulting and joint intersections, led to cutterhead instability and frequent interruptions. The hard and abrasive mineralogy of garnet-rich zones significantly increased tool wear, reducing the operational lifespan of disc cutters. Additionally, unexpected lithological variations, particularly the higher than anticipated percentage of mafic gneiss lithologies, resulted in approximately 35% penetration rate reduction compared to the estimated (Merguerian & Ozdemir, 2003).

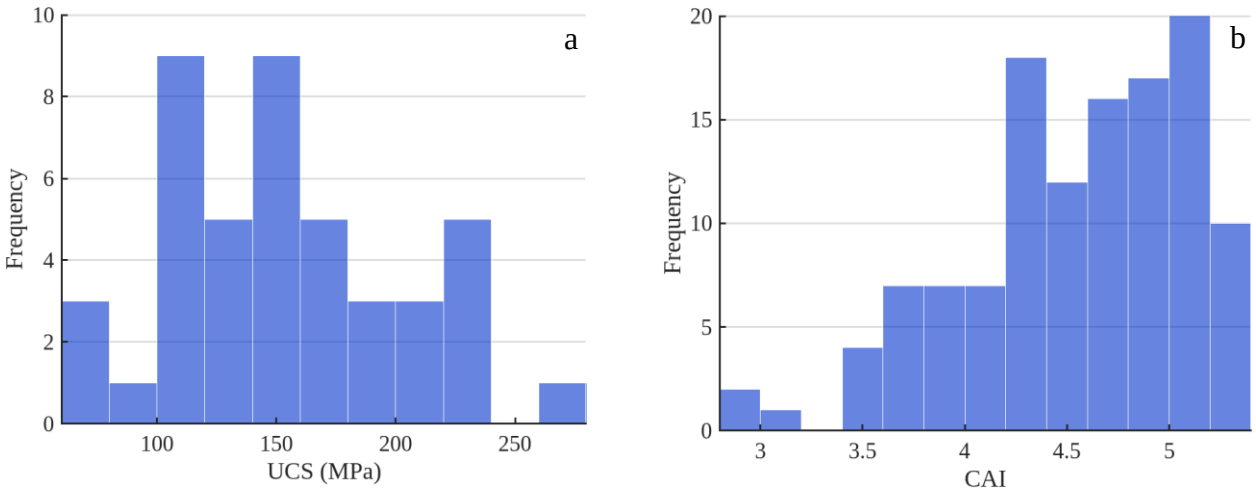

Figure 2.9. Histograms of the UCS (a) and CAI (b) of the Queens Water Tunnel rock samples

CHAPTER 3 – METHODOLOGY

3.1. Overview of Methodology

The methodology adopted in this study builds upon the framework established by Howarth and Rowlands (1987) for quantifying rock texture and its relationship to boreability. The study utilizes an extensive dataset compiled from various sources, focusing on rock texture and mineralogy, physical properties, and operational performance indicators. The dataset originates primarily from investigations during the Queens Water Tunnel TBM project (1996-1999), as detailed in works such as Yagiz (2002) and Merguerian & Ozdemir (2003). The studies by the CSM provided field data on TBM performance, laboratory results for the physical and mechanical properties, and petrographic and mineralogic characteristics of the rock formations that were encountered.

The dataset preparation process involved collecting raw data from these sources, particularly photomicrographs of the rocks' thin sections for further TC computation (Wegrzyn, 1997; Phillipson, 1998) and results of laboratory mechanical tests, standardizing units where necessary, and ensuring consistency across all entries. Special attention was given to the characterization of grain shape, size, and interlocking, which are critical to the Texture Coefficient calculations. The mechanical characterization of selected rock samples was carried out using the laboratory test results provided by the CSM and covering a wide range of properties, including the UCS, BTS, density, CAI, and Brittleness Index (BI). Additionally, TBM operational parameters like ROP, thrust, torque, and power were extracted from the field logs to establish empirical relationships with textural properties. The approach used for TC computation follows the methodology proposed by Howarth and Rowlands (1987), integrating image analysis techniques for accurate quantification. The correlations between TC values and rock mechanical properties and boreability were analyzed statistically, employing regression models to assess the significance and predictive power of the texture coefficient.

3.2. Texture Coefficient Calculation

While the rest of the dataset for analysis and correlative studies is taken directly from the CSM project data with minor changes, mainly unit conversion and selecting only certain data points that correspond to the thin sections of the available rock samples, the texture coefficient data is created fully by the author. The TC computation follows a structured methodology, outlined

initially by Howarth and Rowlands (1987), that involves image analysis, grain boundary tracing, and statistical quantification of rock textural properties. Although the original concept of the Texture Coefficient was introduced in 1987, efforts to modify the TC have remained limited. Kamani and Ajalloeian (2018) presented the Corrected Texture Coefficient, specifically designed for carbonate rocks, focusing on samples with specific strength range and matrix content, assigning a greater influence to the matrix and treating altered and weathered grains as part of the matrix. Their comparison between the original and corrected TC demonstrated improved correlations between engineering properties and texture coefficients, with the corrected TC showing better results. However, similar modifications have not been attempted for igneous or metamorphic rock types. As a result, this study will employ the classic TC, proposed by Howarth and Rowlands (1987), for its analysis. This section provides a step-by-step explanation of the TC calculation procedure.

In the general case, the first step in TC computation involves obtaining high-resolution photomicrographs of thin sections of rock samples. These images must be taken under consistent lighting and focus to ensure reliable analysis. For this study, the sources of the photomicrographs are two reports (Wegrzyn, 1997; Phillipson, 1998) prepared for the Queens Water Tunnel project investigation. The total number of photomicrographs in these two studies is 37, distributed among 27 rock samples; accordingly, some images are associated with a single rock sample, particularly two thin sections per sampling point. While the majority of the photomicrographs satisfy the requirements for TC identification, which is to have at least 20 grains in the observation window for reliable TC calculation, 3 thin sections from the Phillipson (1998) report were rejected due to the low number of grains within the field of view, leaving a total of 24 rock samples that would be used for the analysis in this study. The magnification of these photomicrographs varies from 20x to 50x, making some thin sections much richer in the grain number, which partially influences the TC computation precision. However, since the grain size is not directly involved in the process of TC identification, there is no need to bring each thin section to the same scale. To increase the statistical reliability of the TC calculations, where possible, thin sections were divided into two halves, producing, accordingly, two values of the TC per one sample, the average of which was taken for further analysis. In some cases, as outlined above, two thin sections were available for tracing grain boundaries, and each of them is also divided into two subsections, resulting in a total of four TC values. Overall, the final TC value for each sample is either calculated directly, or is a

mean of two TC values, or is a mean of four TC values, prioritizing the latter. Once the images are selected according to the requirements, they are then processed using image analysis software (ImageJ in the case of this study) to remove noise and trace the grain boundaries.

The image processing with ImageJ software allows for manual outlining of the grain's borders, utilizing personal expertise in optical microscopy, which is especially important for variable and sometimes very complex textures of the metamorphic rocks, while at the same time allowing for automatic calculation of essential geometrical properties required for the TC calculation. As discussed by Howarth and Rowlands (1987), the crucial raw data that should be collected from the photomicrograph analysis include the grain's area (A), perimeter (P), minimum and maximum Feret's diameter (F_{min} and F_{max}), which are the perpendicular distances between two parallel, outer tangents to an object (Figure 3.1) and, therefore, correspond to the grain's 'breadth' and 'length', as well as the angle (F_{angle}) between the maximum Feret's diameter and the horizontal reference line. Figure 3.2 provides an example of capturing data from a thin section using the ImageJ software.

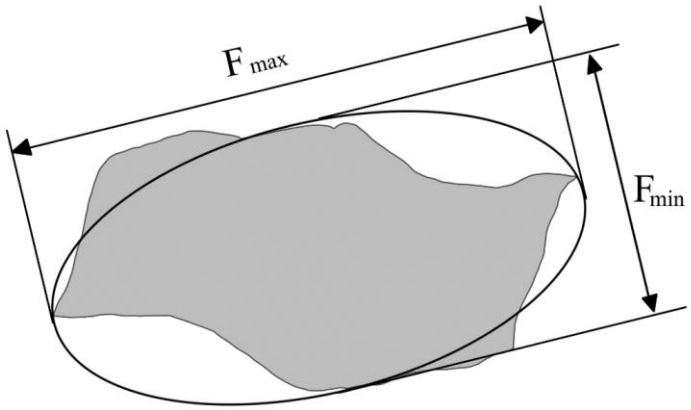

Figure 3.1. Feret's diameter demonstration (after Qui & Pabst, 2023)

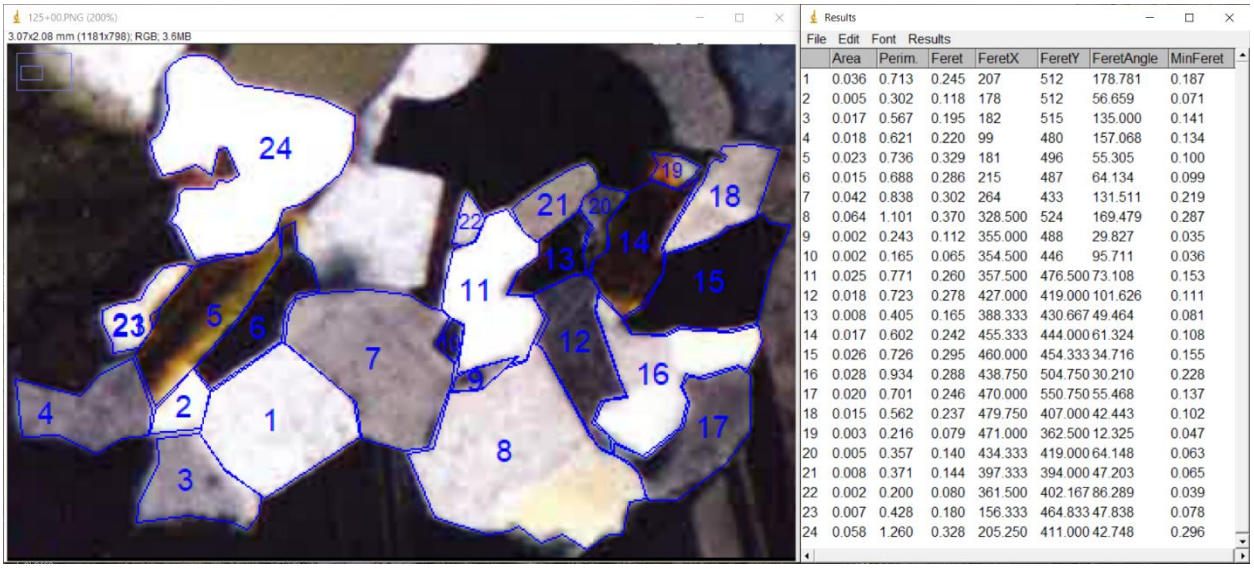

Figure 3.2. ImageJ software interface

Once these five data types are collected for the given thin section, they are transferred to the Excel spreadsheet for further computation. The goal is to extract a single value, TC, for each thin section using the formula proposed by Howarth and Rowlands (1987):

$$TC = AW\left[\left(\frac{N_0}{N_0 + N_I} * \frac{1}{FF_0}\right) + \left(\frac{N_I}{N_0 + N_I}\right) * AR_I * AF_I\right],$$

where TC is the texture coefficient, AW is grain packing weighting, FF_0 is the arithmetic mean of discriminated Form Factors, counted only for circular grains (hence index 0), AR_I is the arithmetic mean of discriminated Aspect Ratios, counted only for elongated grains (hence index I), AF_I is the Angle Factor that quantifies grain orientation, counted only for elongated grains, N_0 is the number of circular grains, which are the grains with Aspect Ratio below a pre-set discrimination level (equal to 2), and N_I is the number of elongated grains, which are the grains with Aspect Ratio above a pre-set discrimination level. Each component of this equation will be addressed in this section.

Grain packing (AW) is a measure of the matrix visible in the thin section photomicrograph and is, therefore, particularly important for sedimentary rocks, in which the matrix contributes a significant amount of the total rock volume. However, in the case of metamorphic rocks, the matrix is usually poorly represented due to the dense granoblastic textures of such rocks. Nevertheless, the intergranular and intragranular alterations, typical for the metamorphic lithologies, could be linked to the AW factor and are counted toward it for this study based on the portion of the

observation window area filled with altered material. For a rock sample completely lacking any matrix (e.g., intact igneous rock), the AW value is equal to 1; the distribution of AW values for this research is between 0.85 and 1.

The number of elongated (N_I) and circular (N_0) grains is identified from the number of grains within the thin section observation window that are fully represented inside its boundaries. Accordingly, if only a portion of the grain is visible inside the thin section image, it is not counted, nor is its boundary traced.

To discriminate between elongated and circular grains, the Aspect Ratio (AR) of grains is calculated, which is the ratio between the maximum and minimum Feret's diameter, and that represents the measurement of grain elongation:

$$AR = \frac{F_{max}}{F_{min}}$$

The Aspect Ratio has two purposes: first, its discriminated mean is directly used in the final TC calculation; and second, it is used for distinguishing between the elongated and circular grains, where the first group is defined as the grains with AR ≥ 2, and the latter group is, accordingly, the grains with AR < 2. This discrimination would be important at later stages of the calculation process, accounting for the higher effect of the elongated grains on the textural cohesion of the studied rocks. For the TC calculation, the arithmetic mean of the Aspect Ratios of all the elongated grains (AR_I) is identified.

$$AR_I = \frac{\sum_{i=1}^{n} AR_i}{n}$$

Next, the Form Factor (FF) is established, which is a measure of a grain's deviation from circularity. It is a function of a grain's area and perimeter and is calculated only for the grains with the Aspect Ratio < 2, or circular grains. Similarly to AR, the arithmetic mean of Form Factors of all the circular grains (FF_0) is used in the final TC equation.

$$FF = 4 * \pi * \frac{A}{P^2}$$

$$FF_0 = \frac{\sum_{i=1}^{n} FF_i}{n}$$

The last component is AF_I, which is the class-weighted mean of the Angle Factors of the elongated grain. It is calculated by a class system applied to the absolute, acute angular differences ($0° \leq \theta \leq 90°$) between every elongated grain. Accordingly, the group of N_I elongated grains will have the number of angular differences equal to $\frac{N_I(N_I-1)}{2}$. Each angular difference is attributed to one of the nine classes that represent the influence of a given angular difference and that are weighted for further calculations (Table 3.1).

Table 3.1. The class weighting system for Angle Factor (AF_I) identification

Class №	Class Range (β)	Weighting (i)
1	$\theta \leq 10°$	1
2	$10° \leq \theta \leq 20°$	2
3	$20° \leq \theta \leq 30°$	3
4	$30° \leq \theta \leq 40°$	4
5	$40° \leq \theta \leq 50°$	5
6	$50° \leq \theta \leq 60°$	6
7	$60° \leq \theta \leq 70°$	7
8	$70° \leq \theta \leq 80°$	8
9	$80° \leq \theta \leq 90°$	9

The Angle Factor is determined by summing the products of class weightings and the proportions of the total angular differences within each class:

$$AF = \sum_{i=1}^{9} \left(\frac{x_i}{\frac{N_1(N_1-1)}{2}} \right) * i,$$

where x_i is the number of angular differences in a given class, and i is a weighting factor and class number. The resulting AF value is divided by 5 to ensure the factor's numerical similarity to the other factors and make its influence on the TC value proportional to that of the rest of the equation's compounds:

$$AF_I = \frac{AF}{5}$$

To demonstrate the TC identification process, an example of a rock sample 1+21_1 thin section will be used. The name of the sample emerges from the station within the tunnel, originally counted in feet and converted to meters. The station 1+21 is the tunnel section 121 m away from the tunnel's start. The underscore accounts for the division of the thin section into two parts (1+21_1 and 1+21_2, respectively). The same naming protocol is used for other thin sections.

The first step is to trace the boundaries of the grains in the thin section photomicrograph using the ImageJ software to collect necessary raw data and count the number of grains that will be used in the analysis. Figure 3.3 represents the original thin section image, and Figure 3.4 illustrates the processed thin sections with the grain boundaries outlined in the software. Note the vertical line that separates the processed thin section into two subsections: the left one, labeled 1+21_1, and the right one, labeled 1+21_2, accordingly. Grains on this vertical line are assigned to one of the subsections based on where most of the grain's area is. The geometrical parameters of all the traced grains are collected using the ImageJ algorithm and then transferred to the Excel spreadsheet, where factors like Aspect Ratio and Form Factor are calculated using the mentioned equations. An example of the data used for the TC identification is given in Table 3.2. The examples of other thin sections, both original and processed, are provided in Appendix A.

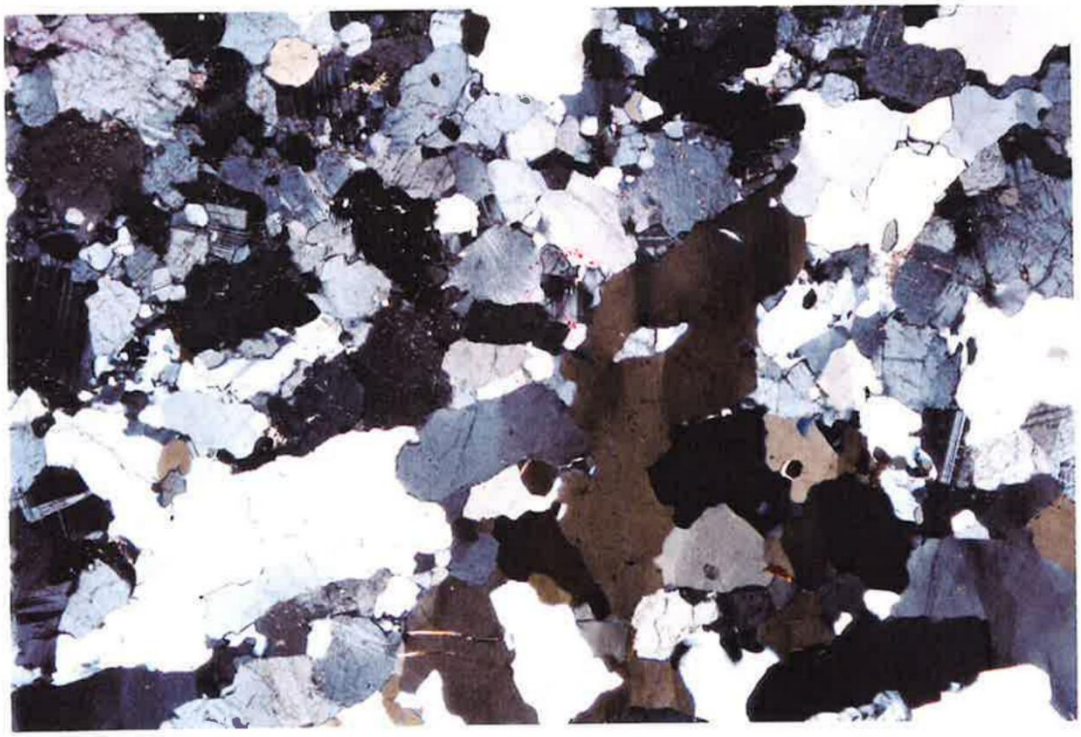

Figure 3.3. Original thin section of 1+21 rock sample (Wegrzyn, 1997)

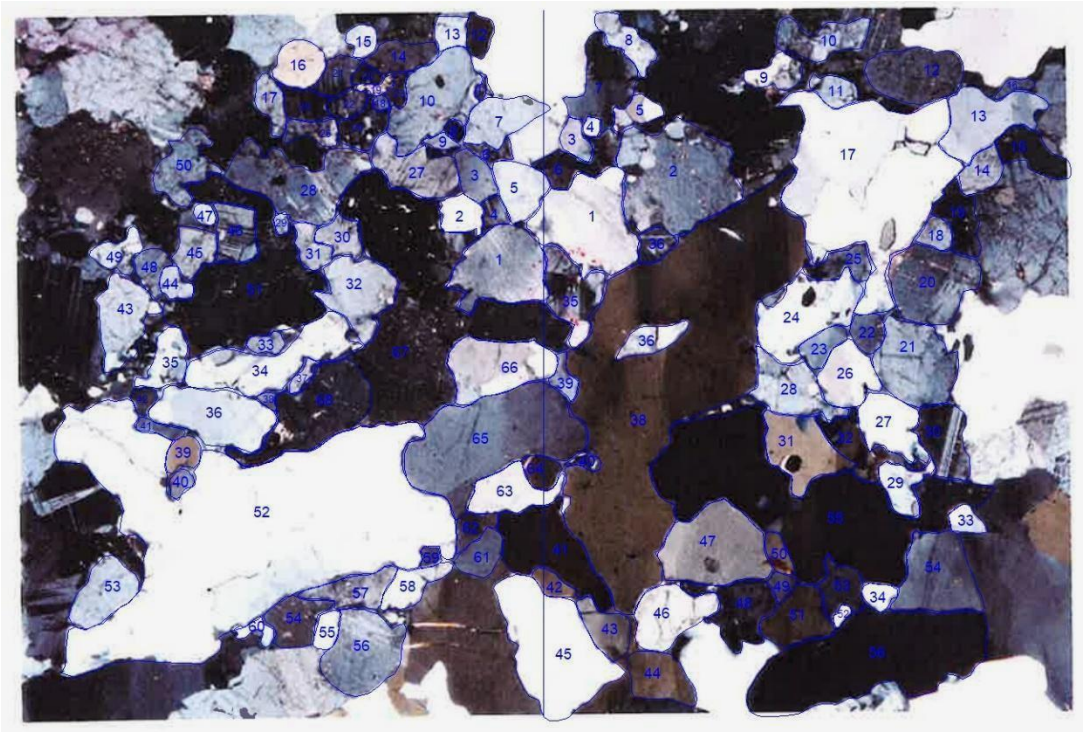

Figure 3.4. Processed thin section of 1+21 rock sample

As seen from the thin section photomicrograph, the observation window is fully packed with grains of minerals, typical for igneous and metamorphic rocks like quartz (white to grey color), plagioclase (dark grey, sometimes with alternating patterns of color stripes due to the polysynthetic twinning), mica (brown color, mainly biotite) and amphibole (dark grey to black with lighter spots). The grains are well-interlocked, relatively fresh, and no significant signs of alteration are visible. Therefore, the AW factor will be assigned as 1 for this sample.

Table 3.2. The TC calculation process (the first 20 lines of the 1+21_1 sample)

	A	P	F_{max}	F_{min}	F_{angle}	AR_i	FF_i
1	0.048	0.969	0.298	0.237	175	1.25738	0.64238
2	0.011	0.443	0.148	0.115	142	1.28696	0.70434
3	0.012	0.432	0.165	0.097	137	1.70103	0.80800
4	0.005	0.328	0.118	0.08	70	1.47500	0.58401
5	0.02	0.544	0.188	0.148	119	1.27027	0.84924
6	0.005	0.412	0.149	0.085	163	1.75294	0.37015
7	0.023	0.659	0.268	0.139	24	1.92806	0.66551
8	0.002	0.182	0.065	0.047	110	1.38298	0.75872
9	0.003	0.25	0.107	0.048	172	2.22917	0.60317
10	0.048	1.004	0.364	0.212	59	1.71698	0.59837
11	0.002	0.234	0.078	0.052	88	1.50000	0.45898
12	0.008	0.357	0.138	0.082	104	1.68293	0.78877
13	0.008	0.364	0.126	0.094	48	1.34043	0.75872
14	0.014	0.515	0.216	0.093	4	2.32258	0.66330
15	0.006	0.314	0.103	0.091	53	1.13187	0.76470
16	0.016	0.464	0.16	0.138	24	1.15942	0.93386
17	0.01	0.452	0.187	0.085	104	2.20000	0.61506
18	0.002	0.146	0.05	0.041	42	1.21951	1.17902
19	0.003	0.286	0.114	0.048	21	2.37500	0.46088
20	0.004	0.246	0.09	0.063	178	1.42857	0.83059

The grains are then grouped into elongated and circular according to the discrimination value of AR = 2. In Table 3.2, the grains numbered 9, 14, 17, and 19 have $AR \geq 2$, and, therefore, are considered elongated; the rest of the grains are, respectively, circular. Thus, when calculating AR_I for the TC equation, the mean AR of grains 9, 14, 17, and 19, as well as the other grains with $AR \geq 2$, will be utilized. Similarly, the FF_0 value is found as the mean of all the FF values of the grains with $AR < 2$.

Next, the AF_I should be addressed by first selecting only the F_{angle} values of the elongated grains. The acute angular differences between all the grains are identified (Table 3.3) and then are weighted using the angle weight class system (Table 3.4). While the majority of grain differences fall into the first three classes (i.e., 0° – 30°), their influence on the final AF value is comparable or even smaller than that of classes with higher weight and fewer grains in them. This reflects the impact of higher angular differences between grains, which increase the rock's cohesion by stronger grain interlocking, maximized at the right angle.

Table 3.3. Acute angular differences for AF_I identification

F_{angle}	20	23	104	172	176	31	26	4	21	16	48	11	174
45	25	22	59	53	49	14	19	41	24	29	3	34	51
20		3	84	28	24	11	6	16	1	4	28	9	26
23			81	31	27	8	3	19	2	7	25	12	29
104				68	72	73	78	80	83	88	56	87	70
172					4	39	34	12	29	24	56	19	2
176						35	30	8	25	20	52	15	2
31							5	27	10	15	17	20	37
26								22	5	10	22	15	32
4									17	12	44	7	10
21										5	27	10	27
16											32	5	22
48												37	54
11													17

Table 3.4. Class weighting for AF_I identification

Angle	Weight	X_i	Angle Factor
$\theta \leq 10°$	1	23	0.25274725
$10° < \theta \leq 20°$	2	17	0.37362637
$20° < \theta \leq 30°$	3	21	0.69230769
$30° < \theta \leq 40°$	4	9	0.3956044
$40° < \theta \leq 50°$	5	3	0.16483516
$50° < \theta \leq 60°$	6	7	0.46153846
$60° < \theta \leq 70°$	7	2	0.15384615
$70° < \theta \leq 80°$	8	4	0.35164835
$80° < \theta \leq 90°$	9	5	0.49450549
AF			**3.34065934**

The last step is to put all the identified parameters together into the TC equation. Table 3.5 shows the final factors and the resulting TC value of 1.503, which is within the typical range for metamorphic rocks according to Howarth and Rowlands (1987). This way, TC is calculated for 24 sampling points to be included in the dataset.

Table 3.5. TC factors and calculation

AW	N_0	N_I	FF_0	AR_I	AF_I	**TC**
1	54	14	0.68008	2.43765	0.6681319	**1.503**

The distribution of TC values for this study is provided in Figure 3.5, indicating that the majority of rock samples fall into the range between 1.4 and 1.8, which corresponds to the expected results for metamorphic rocks based on the previous studies (Howarth & Rowlands, 1987; Azzoni et al., 1996). This distribution suggests that the majority of the samples have moderately low to moderate textural complexity according to the framework established by Howarth & Rowlands (1987). Lower TC values generally correspond to rocks with simpler, less interlocked textures, typically found in more drillable, less mechanically resistant rocks. Higher TC values (above TC = 2), though less common in this dataset, are indicative of rocks with more complex, interlocked textures, which are known to exhibit higher resistance to crack propagation and lower drillability.

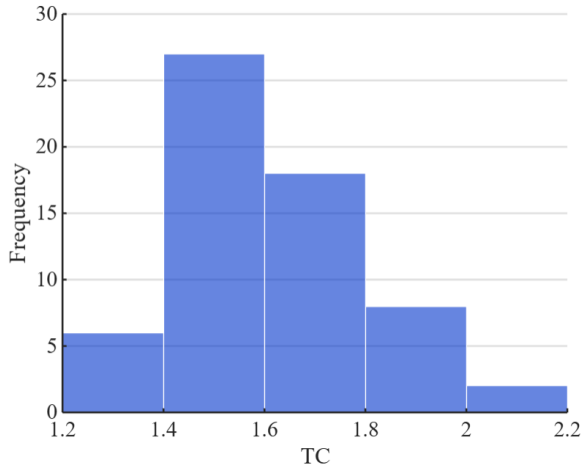

Figure 3.5. Histogram of TC values

3.3. Dataset Preparation

The dataset for this research was created using TC values from the thin section images, results from laboratory tests on the mechanical and physical properties of rock samples done by the CSM, rock mass properties collected within the excavation, and data on TBM performance during tunnel excavation taken from field logs, focusing on the areas where the rock samples were collected.

The original tests and recordings of the field TBM data were done in the U.S. and, therefore, mainly utilize the imperial unit system. To maintain consistency in this study, all the units were converted to the International System of Units, SI. Thus, the units used in the dataset include MPa for the UCS and BTS; kN/mm for the Brittleness Index; m/hr for the ROP; kN for the Thrust; kW for the Cutterhead Power; and kN·m for the Cutterhead Torque.

Table 3.6 summarizes the dataset components that will be used for the statistical analysis, which is based on the number of available thin section images, that is, 24. Thus, for the majority of the parameters, the number of values is also 24. In the case of some physical properties, however, the values for certain rock samples were not available in the initial datasets (e.g., BTS, BI). These parameters were still added to the final dataset but had lower priority for the statistical analysis to maximize the number of lines and, therefore, the reliability of the study.

Table 3.6. Dataset components

TC Factors	Physical Properties	Rock Mass Properties	Machine Properties
Tunnel Station (m)	UCS (MPa)	Alpha Angle (degree)	ROP (m/hr)
Rock Sample	BTS (MPa)	Fracture Spacing (m)	Net Thrust (kN)
Rock Type	Density (kN/m^3)		Cutterhead Power (kW)
Average TC	BI (kN/mm)		Cutterhead Torque (kN·m)
Mineralogy	CAI		
	Mohs Hardness		

Accordingly, the compiled dataset covers key textural, physical, mechanical, and operational parameters that will be utilized in the analysis for model development. While TC was defined and thoroughly explained in the previous section, the other parameters also require proper definition, which will be done group by group as outlined in Table 3.6.

Mineralogy refers to the mineralogical composition of the rock samples, specified in the reports on the thin section description (Wegrzyn, 1997; Phillipson, 1998). In the case of the rocks of the Queens Water Tunnel complex, the main minerals include quartz, plagioclase, mica, amphibole, garnet, and feldspar. The studies by Tiryaki and Dikmen (2005) and Ghosh et al. (2012) highlight the importance of rock mineralogical composition on the response to mechanical impact, particularly a degrading effect of feldspar on the rock's strength, which is likely linked to the low resistance of feldspar to the weathering, often resulting in its partial transition to clay minerals (e.g., kaolinite). On the other hand, abrasive minerals like quartz and garnet are known for their effect on increased tool wear and, therefore, drops in the advance rate of the machine. The quartz and garnet content are summarized together with average TC values and rock types in Table 3.7, and the histograms are provided in Figure 3.6.

Table 3.7. Texture, Mineralogy, and Rock Type data

№	Station, m	TC	Quartz, %	Garnet, %	Rock Type
1	121	1.77	60	0	Quartz diorite
2	189	1.68	59	4	Quartz diorite
3	240	1.54	7	2	Pyroxene-hornblende gneiss
4	320	1.71	4	19	Pyroxene-garnet-hornblende gneiss
5	366	1.55	19	16	Pyroxene-hornblende-garnet gneiss
6	386	1.45	29	19	Pyroxene-hornblende-garnet gneiss
7	488	1.42	10	9	Garnet-hornblende-pyroxene gneiss
8	610	1.52	52	6	Pyroxene bearing garnet-hornblende-quartz gneiss
9	652	1.74	27	17	Pyroxene-garnet-hornblende-quartz gneiss
10	2076	1.62	25	15	Garnet-hornblende gneiss
11	2152	1.55	15	30	Biotite-hornblende-garnet gneiss
12	2195	1.62	25	2	Garnet-bearing biotite-quartz gneiss
13	2225	1.50	10	12	Biotite-garnet-hornblende gneiss
14	2316	1.50	25	5	Hornblende-bearing garnet-biotite-quartz gneiss
15	2560	1.82	8	20	Garnet-hornblende gneiss
16	2682	1.30	0	0	Biotite-hornblende gneiss
17	2804	1.62	20	8	Garnet-biotite gneiss
18	3048	1.85	25	20	Hornblende-biotite-garnet-quartz gneiss
19	3170	1.48	30	10	Garnet-biotite-quartz gneiss
20	3292	1.68	17	10	Garnet-hornblende gneiss
21	3414	1.61	0	10	Garnet-hornblende gneiss
22	3536	1.58	15	0	Biotite-hornblende gneiss
23	3658	1.77	30	15	Hornblende-bearing biotite-garnet-quartz gneiss
24	3810	1.50	23	2	Garnet-bearing biotite-hornblende-quartz gneiss

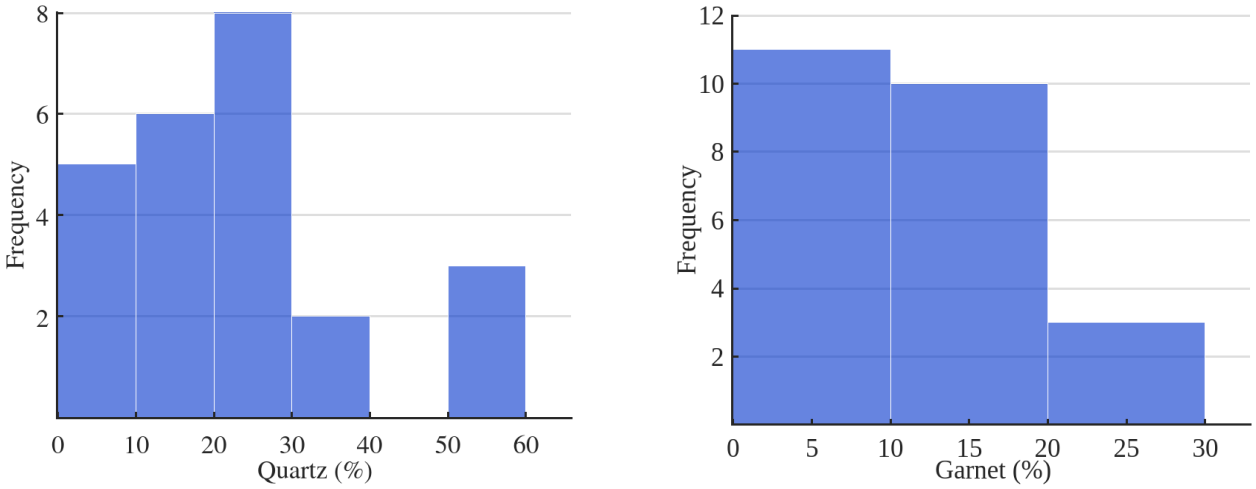

Figure 3.6. Histograms of the Quartz and Garnet content data

The quartz content histogram shows that most samples have quartz percentages between 10% and 30%. A smaller number of samples exhibit either low (<10%) or relatively high (>50%) quartz contents. This distribution suggests that the majority of the studied rocks are intermediate in silica content, consistent with granitic gneisses, where quartz occurs as a major rock-forming mineral. The garnet content histogram indicates a more clustered distribution, with the majority of samples containing between 0% and 20% garnet. The presence of garnet, even at relatively low concentrations, is significant given garnet's contribution to increased rock hardness and abrasivity. Garnet-bearing rocks, common in metamorphic terrains such as those observed in the Queens Water Tunnel project terrain, are typically associated with higher rock abrasiveness and greater tool wear rates during excavation.

Next, the physical properties of the dataset will be defined. UCS is a fundamental mechanical property representing the maximum axial compressive stress a rock specimen can withstand before failure. It is a critical input for performance models such as those developed by CSM and NTNU. High UCS values generally denote stronger, more resistant rocks that require high thrust and torque from TBMs to penetrate the rock. In the context of rock mechanics and excavation, UCS is not only indicative of overall intact rock strength but also defines the selection of cutter types and machine operational settings (Hassanpour et al., 2011).

BTS quantifies the indirect tensile strength of rocks, derived from diametral loading of disc-shaped specimens. It is an essential factor in understanding rock brittleness and fracture behavior under TBM cutting forces. Rocks with low BTS are more susceptible to tensile crack propagation, potentially enhancing chipping and fragmentation during excavation. In studies such as Bilgin et al. (2016), BTS has been shown to correlate with penetration rate and cutter consumption.

Rock density reflects the mass per unit volume, influencing the mechanical response under load and during dynamic excavation processes. Though not always directly correlated with TBM performance, it provides complementary data for estimating specific energy and evaluating rock integrity.

The Brittleness Index, as defined by Yagiz et al. (2009), reflects the tendency of a rock to fracture rather than deform plastically. It is commonly computed from UCS and BTS values. A higher BI typically indicates more efficient chipping and fragmentation during TBM operation, often translating to increased penetration rates and reduced specific energy. Yagiz (2009) emphasized the importance of BI in TBM performance prediction models, highlighting its role in optimizing operational parameters and estimating machine penetration rates.

Hardness quantifies the surface resistance of a rock to physical impact. It is considered an indirect indicator of rock strength and wear potential and is usually identified with tools like the Shore scleroscope or Schmidt hammer. In this study, however, hardness refers to the weighted average Mohs hardness of the minerals comprising a given rock. Tiryaki and Dikmen (2005) and Tumac et al. (2017) have shown correlations between rock hardness and the specific energy required for chisel tool performance, particularly in natural stone cutting.

CAI measures the abrasive potential of rock against cutting tools, directly impacting cutter wear and maintenance intervals. A higher CAI corresponds to greater abrasivity, leading to increased operational expenses and lower efficiency. According to Ribacchi & Lembo Fazio (2005), CAI is one of the most influential factors affecting TBM cutter consumption and is often included in classifications of rock mass boreability. The physical properties as well as average TC data for this research are given in Table 3.8, and the histograms are provided in Figure 3.7.

Table 3.8. Physical Properties data

№	Station, m	UCS, MPa	BTS, MPa	Density, kN/m^3	BI, kN/mm	Mohs Hardness	CAI
1	121	148.34	-	2.64	-	6.40	4.55
2	189	221.59	11.31	2.69	53.60	6.37	5.08
3	240	110.69	-	3.06	48.90	5.85	4.07
4	320	153.80	7.08	2.96	59.96	6.09	3.94
5	366	144.42	-	2.86	65.43	6.33	5.11
6	386	166.77	-	2.79	69.41	6.22	4.37
7	488	119.65	6.52	3.01	-	6.23	4.65
8	610	142.14	-	2.65	43.21	6.68	4.44
9	652	147.33	10.50	2.72	54.74	6.42	4.57
10	2076	154.51	10.34	3.03	38.67	6.20	5.03
11	2152	128.20	10.45	2.77	38.82	6.20	4.75
12	2195	118.60	7.49	2.59	48.90	6.10	5.17
13	2225	152.82	9.11	2.88	-	5.80	5.04
14	2316	64.56	10.16	2.98	34.19	5.80	4.32
15	2560	77.63	9.12	2.95	26.71	5.70	3.56
16	2682	104.76	10.40	2.89	-	5.30	3.12
17	2804	163.72	10.07	2.79	21.05	5.30	4.30
18	3048	135.71	9.75	2.91	41.26	6.20	4.58
19	3170	118.89	9.03	2.70	37.80	6.30	4.58
20	3292	185.68	13.17	2.80	34.94	6.30	5.00
21	3414	100.73	9.56	2.72	13.99	6.10	2.98
22	3536	129.96	13.92	2.70	27.69	5.60	4.71
23	3658	150.26	9.32	2.79	45.33	6.20	4.65
24	3810	121.96	6.94	2.70	38.60	5.80	4.80

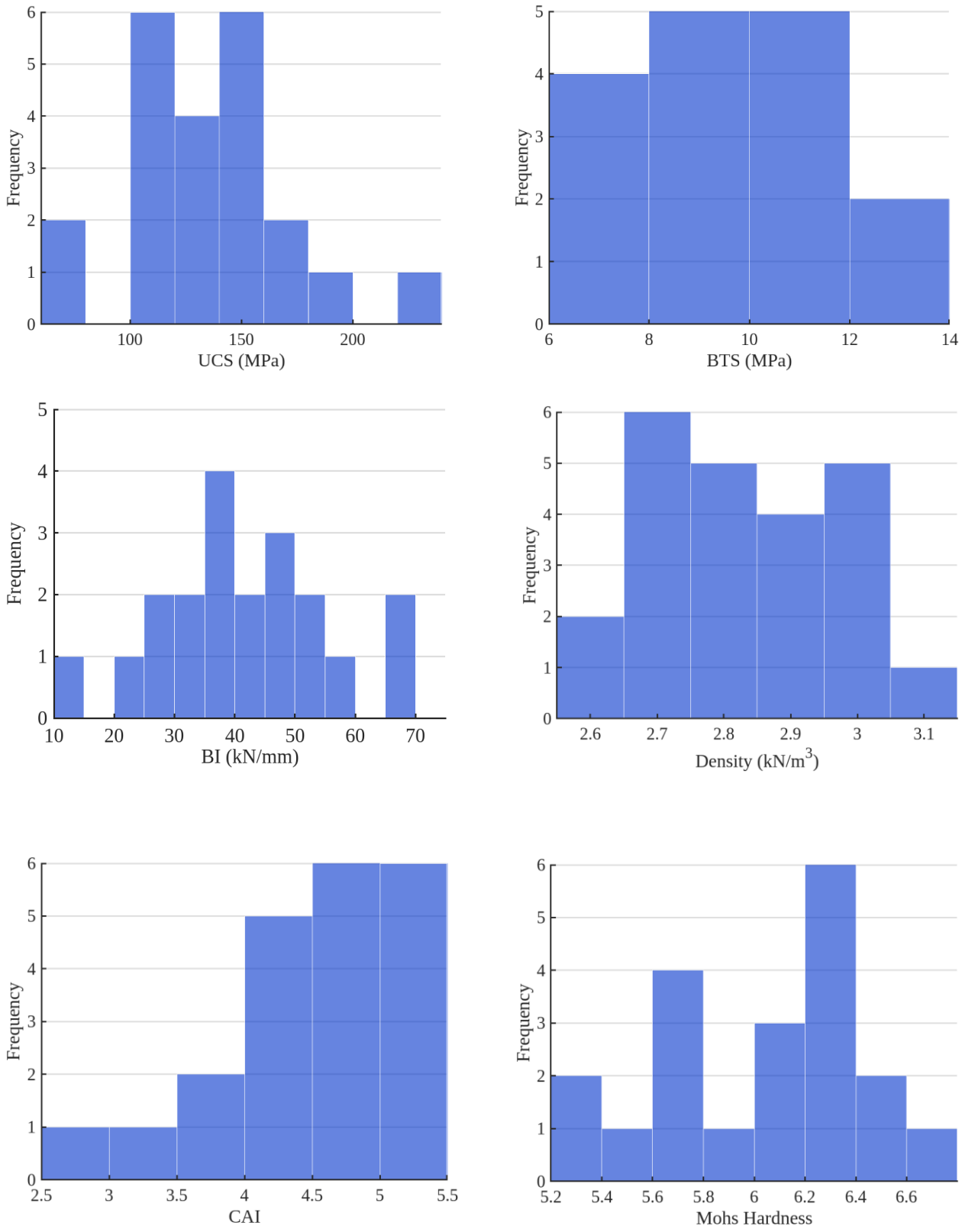

Figure 3.7. Histograms of the Physical Properties

The UCS values show a slight right-skew, with most samples concentrated between 100 and 160 MPa, suggesting a moderately strong rock mass overall. The BTS distribution is relatively uniform between 8 and 12 MPa, indicating variability in tensile resistance across the samples. The Brittleness Index values are spread fairly evenly between 20 and 60 kN/mm, with a concentration around 35-50 kN/mm, reflecting a predominance of rocks with high to very high brittleness, which can significantly influence cutter wear and penetration rates. Density shows a narrower distribution, mainly clustering around 2.7 to 3.0 kN/m^3, typical for crystalline rocks, suggesting relatively consistent material behavior. CAI values are skewed toward the higher end (4.5-5.0), indicating that most rocks are highly abrasive, which is critical for assessing cutter consumption. Lastly, Mohs hardness values peak around 6.0-6.4, implying that the majority of samples have moderate to high hardness, another factor contributing to TBM tool wear. The distribution of these properties suggests a rock mass environment where both penetration performance and cutter wear will be highly sensitive to local variations in strength and abrasivity.

The rock mass properties belong to the next group of the dataset components. The Alpha Angle refers to the orientation of planes of weakness within the rock, most commonly the angle between the cutting trajectory of the TBM and pre-existing geological structures such as bedding, foliation, or joint sets, depending on the lithology. This angle significantly influences TBM performance because certain alignments facilitate chipping and crack propagation, while others increase the resistance and tool wear. According to Salimi et al. (2017), penetration rates are typically higher when discontinuities intersect the tunnel face at angles from 45° to 90°, depending on the rock mass characteristics, particularly the spacing of joint sets. At very low or very high alpha angles, resistance to excavation increases, potentially causing cutter bouncing and reduced efficiency.

Fracture spacing denotes the average distance between adjacent discontinuities in the rock mass. It serves as an essential parameter in characterizing rock mass quality and is inversely proportional to the degree of fragmentation. Close-spaced fractures often enhance TBM penetration due to the rock's predisposition to break into smaller blocks; however, excessively fractured zones can lead to instability and clogging issues. On the other hand, wide fracture spacing indicates more intact rock, requiring greater cutter force and energy input. The rock mass properties data is summarized in Table 3.9 and Figure 3.8.

Table 3.9. Rock Mass Properties data

№	Station, m	Alpha Angle, °	Fracture Spacing, m	№	Station, m	Alpha Angle, °	Fracture Spacing, m
1	121	12.00	0.4	13	2225	47.73	15
2	189	37.83	15	14	2316	-	0.1
3	240	24.89	0.8	15	2560	66.84	0.2
4	320	38.19	15	16	2682	62.39	0.2
5	366	28.88	0.8	17	2804	22.91	1.6
6	386	70.00	0.2	18	3048	-	15
7	488	32.00	0.8	19	3170	15.24	1.6
8	610	43.17	1.6	20	3292	31.73	1.6
9	652	-	0.4	21	3414	49.91	0.2
10	2076	62.01	0.8	22	3536	47.38	15
11	2152	36.99	15	23	3658	80.52	0.2
12	2195	-	1.6	24	3810	-	1.6

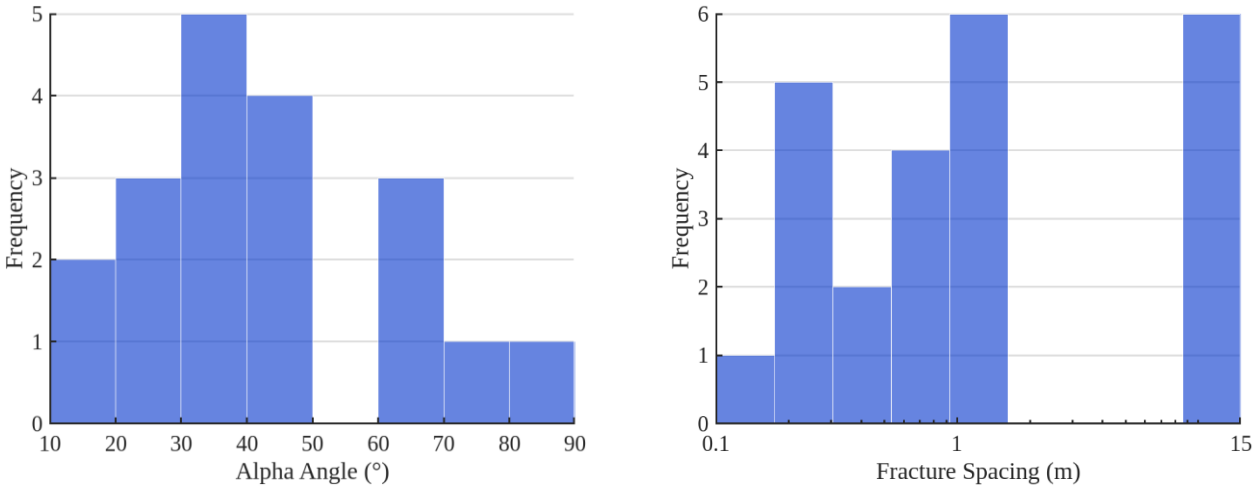

Figure 3.8. Histograms of the Rock Mass Properties

Alpha angle values are mostly clustered between 20° and 50°, indicating a general prevalence of moderately inclined joint sets, which can influence rock block stability and cutterhead interactions. Higher alpha angles above 60° are less common but still present, potentially contributing to improved fracturing as mentioned before. Fracture spacing displays a bimodal pattern, with peaks at around 0.5-1.5 meters and another group at 15 meters. The dominance of wider spacings suggests that large intact rock blocks are common, generally favorable for TBM advance rates. However, the presence of closely spaced fractures suggests potential excavation instabilities and operational obstructions.

Finally, the TBM operational parameters will be specified. The Rate of Penetration (ROP) represents the average linear distance the TBM advances per revolution of the cutterhead or per unit of time. It is a critical indicator of TBM performance, influenced by both machine settings (thrust, torque, cutter configuration) and geological conditions. Higher ROP typically suggests efficient excavation, although it may also correlate with increased cutter wear in abrasive rocks. Many empirical models – including those by NTNU and CSM – rely on ROP as a central variable in evaluating excavation productivity (Rostami & Ozdemir, 1993; Bruland, 1998).

Thrust force is the axial load applied by the TBM's hydraulic jacks to advance the cutterhead against the tunnel face, and it is one of the most influential machine parameters affecting penetration rate, cutter engagement, and rock fragmentation efficiency. In TBM performance modeling, it is important to distinguish between total and net thrust. Total thrust refers to the full axial force generated by the TBM's main cylinders during excavation, whereas net thrust represents the effective portion of this force that contributes directly to rock cutting. Net thrust is calculated by subtracting losses due to shield–rock friction and towing resistance from the total thrust.

Cutterhead power is the total installed power delivered to the cutterhead, combining torque and RPM. It defines the energy input capacity of the TBM. Cutterhead power is used to calculate specific energy, which is the amount of energy consumed per unit volume of excavated rock. Lower SE values correspond to more efficient excavation (Bilgin et al., 2016).

Torque is the rotational force applied by the TBM to overcome rock resistance during cutterhead rotation. High torque values indicate harder or more interlocked rock masses and may signal the need for increased thrust or reduced advance rate. Torque is closely linked to specific energy calculations and is a key parameter in TBM performance prediction and cutterhead design (Schlicke et al., 2024). Table 3.10 and Figure 3.9 demonstrate the machine parameters data selected for this study.

Table 3.10. Machine Parameters data

№	Station, m	ROP, m/hr	Net Thrust, kN	Cutterhead Power, kW	Cutterhead Torque, kN·m
1	121	1.52	12787.79	810.16	953.59
2	189	2.86	16540.70	1906.78	2191.03
3	240	2.59	14194.60	1492.00	1715.22
4	320	1.24	14060.21	617.69	712.95
5	366	1.12	14522.87	578.90	661.90
6	386	2.01	10546.96	824.33	943.77
7	488	1.31	15527.54	892.96	1019.83
8	610	1.42	13498.70	794.49	915.19
9	652	1.97	17688.62	1147.63	1319.61
10	2076	1.65	15604.91	1118.25	1286.30
11	2152	1.37	16961.65	985.47	1133.29
12	2195	1.85	16815.68	1147.35	1319.88
13	2225	0.78	17152.31	691.54	792.66
14	2316	1.53	9154.57	641.56	740.43
15	2560	2.95	14385.52	1406.21	1619.92
16	2682	2.70	13226.25	1153.32	1409.63
17	2804	1.62	16721.12	1050.37	1205.53
18	3048	2.06	15743.96	1230.15	1411.54
19	3170	2.02	16154.40	1167.49	1338.86
20	3292	1.57	15696.63	1057.08	1219.28
21	3414	1.93	13034.37	1065.29	1222.97
22	3536	1.95	17366.78	1297.29	1490.12
23	3658	2.34	14358.26	1290.58	1481.63
24	3810	1.80	18105.12	1219.22	1402.99

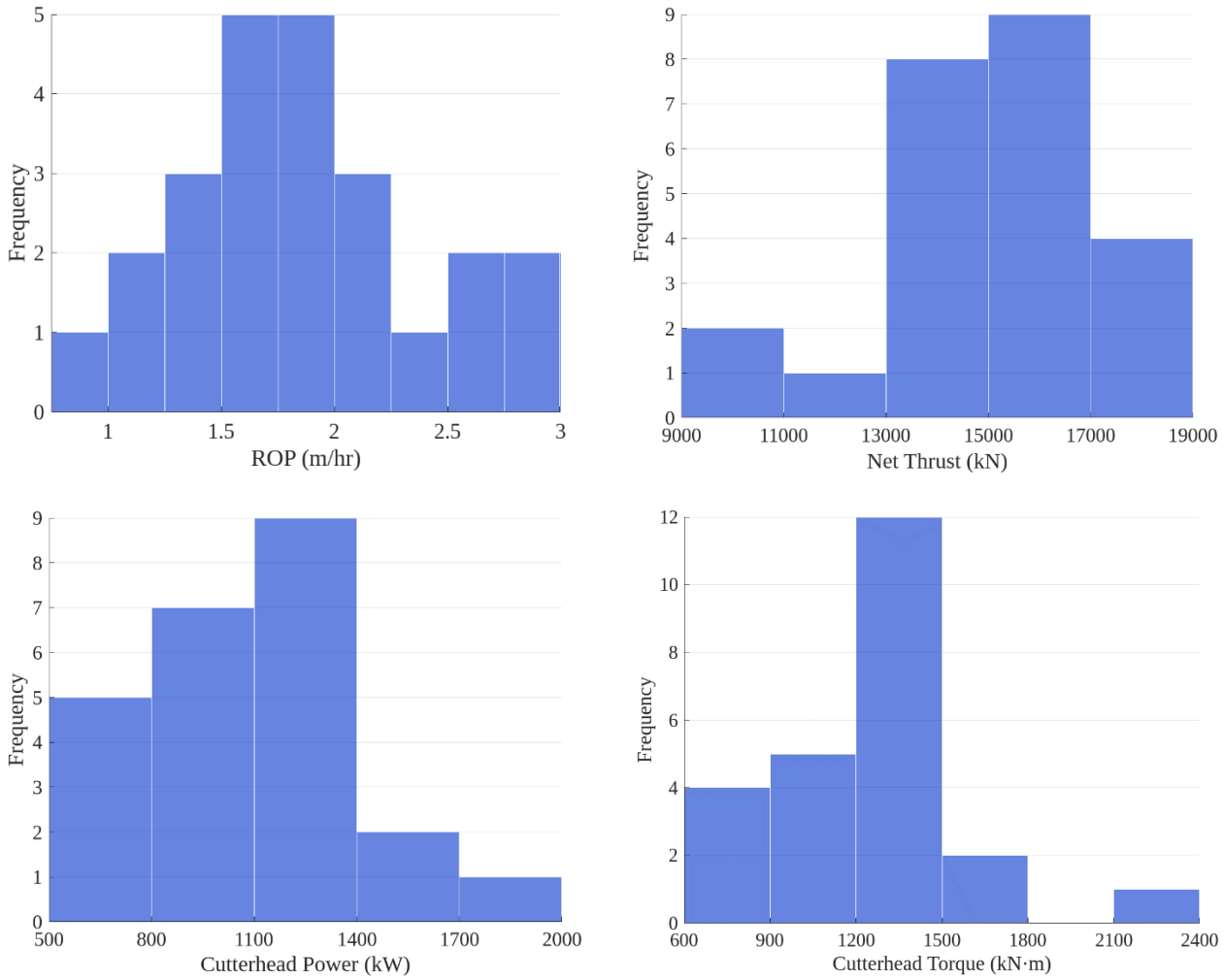

Figure 3.9. Histograms of the Machine Parameters

The ROP is mainly distributed at around 1.5-2.0 m/hr, suggesting low to moderate excavation speeds across the studied sections, aligning with the previously discussed drop in the real advance rate as opposed to the anticipated. Net thrust values are clustered between 13,000 and 17,000 kN, reflecting relatively high and consistent thrust demands typical for hard rock TBM operations. Cutterhead power is primarily concentrated between 800 and 1400 kW, indicating that the machine operated predominantly within a mid-to-high power range. Cutterhead torque shows a strong peak at around 1200-1500 kN·m, suggesting that while torque demands were substantial, extremely high torques were less frequent.

Table 3.11 presents the descriptive statistics for the dataset compiled in this study, including up to 24 observations across a range of physical, mechanical, and machine parameters relevant to TBM performance. The table summarizes the minimum, maximum, mean, and standard deviation for each variable, offering a general overview of the dataset's distribution and variability. Next, the statistical analysis in the SPSS software will be performed to establish correlations and build the model for TBM performance prediction using linear and non-linear regression techniques.

Table 3.11. Dataset descriptive statistics

Parameter	N	Minimum	Maximum	Mean	Std. Deviation
Average TC	24	1.30	1.85	1.60	0.14
UCS, MPa	24	64.56	221.59	135.95	33.34
BTS, MPa	19	6.52	13.92	9.70	1.91
Density, kN/m^3	24	2.59	3.06	2.82	0.13
BI, kN/mm	20	13.99	69.41	42.16	14.24
Mohs Hardness	24	5.30	6.68	6.06	0.35
CAI	24	2.98	5.17	4.47	0.59
Fracture Spacing, m	24	0.10	15.00	4.36	6.30
Alpha Angle, °	19	12.00	80.52	42.66	19.04
ROP, m/hr	24	0.78	2.95	1.84	0.55
Net Thrust, kN	24	9154.57	18105.12	14993.73	2219.53
Cutterhead Power, kW	24	578.90	1906.78	1066.09	308.25
Cutterhead Torque, kN·m	24	661.90	2191.03	1229.50	355.15

CHAPTER 4 – RESULTS

4.1. Outlier Detection and Removal

To improve the reliability and robustness of the statistical analysis, it is essential to identify and appropriately manage outliers within the dataset. Outliers can disproportionately influence correlation and regression results, leading to misleading interpretations and reduced model accuracy (Montgomery, 2013). Despite containing only 24 lines, the dataset still has the potential to host some critical outliers, which would significantly affect the outcomes of the statistical analysis. Thus, to ensure that the dataset accurately represents the geomechanical behavior of the studied rocks, an objective and systematic method was applied for outlier detection and evaluation, while prioritizing keeping as many data lines as possible.

To identify and justify the removal of outliers from the dataset, the Interquartile Range (IQR) method was used (Hubert & Vandervieren, 2007). This method defines outliers as data points that fall significantly outside the central spread of the data distribution. For each continuous variable, the first quartile (Q1) and third quartile (Q3) were computed. Q1 represents the 25th percentile of the data, meaning 25% of the values lie below it, while Q3 represents the 75th percentile, where 75% of the values lie below. The IQR is then calculated as the difference between Q3 and Q1 (IQR = Q3 − Q1), representing the middle 50% of the dataset. A data point is considered an outlier if it lies below Q1 − 1.5 × IQR or above Q3 + 1.5 × IQR.

This calculation was applied independently to each selected parameter to identify data points that notably deviate from the typical distribution. Before this step, the preliminary assessment of variables was performed to identify the most promising properties for the analysis and limit further work to them (see more in Chapter 4.3). TC is included in this list as this is the core aspect of the study; additionally, using simple regression in SPSS, the following parameters were selected based on their correlation with ROP: UCS, CAI, Alpha Angle, and Cutterhead Power (CP). For each row in the dataset, a point was assigned for every parameter (including ROP) where the value was classified as an outlier. These points were then summed across all parameters to generate an “Outlier Score” for each observation, indicating how many variables simultaneously classified that line as an outlier (Table 4.1). This process revealed that one particular observation, corresponding to Line 2 of the original dataset (Station 189 m), exhibited outlier characteristics in three separate parameters: ROP, CP, and UCS.

Specifically, this line showed a very high ROP value (2.86 m/hr), an unusually high CP (1907 kW), and one of the highest UCS values (222 MPa) – marked in bold in Table 4.1. The simultaneous deviation in multiple key parameters suggests that this observation represents a fundamentally different geomechanical or operational scenario compared to the rest of the dataset. Such a point has the potential to significantly influence statistical models and distort general trends, particularly in regression or variance-based analyses (Montgomery, 2013). Therefore, its removal is statistically justified to maintain the homogeneity and representativeness of the dataset and to ensure the reliability of subsequent analytical results.

Table 4.1. Outlier detection

№	Station, m	ROP, m/hr	TC	UCS, MPa	CAI	α, °	CP, kW	Outlier Score
1	121	1.52	1.77	148	4.55	12	810	0
2	189	**2.86**	1.68	**222**	5.08	38	**1907**	3
3	240	2.59	1.54	111	4.07	25	1492	0
4	320	1.24	1.71	154	3.94	38	618	0
5	366	1.12	1.55	144	5.11	29	579	0
6	386	2.01	1.45	167	4.37	70	824	0
7	488	1.31	1.42	120	4.65	32	893	0
8	610	1.42	1.52	142	4.44	43	794	0
9	652	1.97	1.74	147	4.57	-	1148	0
10	2076	1.65	1.62	155	5.03	62	1118	0
11	2152	1.37	1.55	128	4.75	37	985	0
12	2195	1.85	1.62	119	5.17	-	1147	0
13	2225	0.78	1.50	153	5.04	48	692	0
14	2316	1.53	1.50	**65**	4.32	-	642	1
15	2560	2.95	1.82	**78**	3.56	67	1406	1
16	2682	2.7	**1.30**	105	3.12	62	1153	1
17	2804	1.62	1.62	164	4.3	23	1050	0
18	3048	2.06	1.85	136	4.58	-	1230	0
19	3170	2.02	1.48	119	4.58	15	1167	0
20	3292	1.57	1.68	186	5	32	1057	0
21	3414	1.93	1.61	101	**2.98**	50	1065	1
22	3536	1.95	1.58	130	4.71	47	1297	0
23	3658	2.34	1.77	150	4.65	81	1291	0
24	3810	1.8	1.50	122	4.8	-	1219	0

4.2. ANOVA Test

To statistically assess the influence of selected rock and machine parameters on TBM penetration performance, an Analysis of Variance (ANOVA) test was conducted. ANOVA is a fundamental statistical method used to evaluate whether there are significant differences in the mean values of a continuous dependent variable across multiple categorical groups of an independent variable. In its one-way form, ANOVA measures the ratio of between-group variance to within-group variance, producing two key outputs: the F-statistic and the p-value. The F-statistic quantifies how much of the variability in ROP can be attributed to differences between groups defined by a categorical predictor. The p-value, derived from the F-distribution, indicates the statistical significance of these differences; a p-value below a commonly accepted threshold ($p < 0.05$ or 0.01) suggests that at least one group mean differs meaningfully from the others (Montgomery, 2013). In this study, the dependent variable is the Rate of Penetration, while the independent variables are parameters like TC, UCS, CAI, Alpha Angle, and CP.

Before applying ANOVA, it was necessary to appropriately categorize the continuous variables into discrete groups. Initially, automated binning techniques such as equal-width division and quantile-based grouping were explored. Although these methods maximize statistical sensitivity by creating relatively balanced groups, they often produce arbitrary bin edges (e.g., 142.66 MPa for UCS or 3.73 for CAI), making the results difficult to interpret from an engineering perspective.

To address these issues, a custom binning strategy was adopted based on domain-specific knowledge, standard classification frameworks, and observed data distributions (Table 4.2). This approach allowed the groupings to be both statistically meaningful and supported by engineering judgment. The final groupings were defined as follows:

- TC: 1.30–1.50 (Low), 1.50–1.70 (Medium), and 1.70–1.90 (High), following empirical ranges used in texture-based boreability models taking into account the TC distribution within the dataset (Ozturk & Nasuf, 2013; Tumac et al., 2017).
- UCS: 60–100 MPa (Low), 100–150 MPa (Medium), and 150–190 MPa (High), based on the strength variability across the studied rocks.

- CAI: 2.9–3.8 (Low), 3.8–4.6 (Medium), and 4.6–5.4 (High), accounting for the general high rock abrasiveness of the dataset as concluded from the CAI histogram and supported by quartz and garnet content in rocks.
- Alpha Angle**:** 0–30° (Low), 30–60° (Medium), and 60–90° (High), consistent with classifications used in joint orientation and rock mass behavior studies.
- CP: 550–900 kW (Low), 900–1200 kW (Medium), and 1200–1500 kW (High), corresponding to the distribution of operational data from the studied tunnel section.

Table 4.2. Variables grouping for the ANOVA test

Parameter	Low	Medium	High
TC	$1.30 \leq TC < 1.50$	$1.50 \leq TC < 1.70$	$1.70 \leq TC < 1.90$
UCS, MPa	$60 \leq UCS < 100$	$100 \leq UCS < 150$	$150 \leq UCS < 190$
CAI	$2.90 \leq CAI < 3.80$	$3.80 \leq CAI < 4.60$	$4.60 \leq CAI < 5.40$
α, °	$0 \leq \alpha < 30$	$30 \leq \alpha < 60$	$60 \leq \alpha \leq 90$
CP, kW	$550 \leq CP < 900$	$900 \leq CP < 1200$	$1200 \leq CP \leq 1500$

With these custom groupings established, one-way ANOVA was applied to each parameter to assess its individual effect on ROP. The F-statistic and corresponding p-value were calculated for each variable, providing a measure of whether the group means differed significantly (Table 4.3). The results indicated that CP, CAI, and Alpha Angle produced statistically significant p-values ($p = 0.0011$, 0.0127, and 0.0172, respectively), suggesting that the mean ROP values vary meaningfully across the defined low, medium, and high categories for these parameters. This confirms that machine power, rock abrasivity, and geological orientation features have a notable effect on TBM performance. On the other hand, TC and UCS did not yield statistically significant results ($p = 0.2218$ and 0.1370, respectively) under the current grouping structure. This outcome suggests that, at least within the studied dataset, rock texture and compressive strength alone do not produce distinct variations in ROP when categorized in this manner. Nevertheless, both parameters may still play a secondary or interactional role when considered alongside other influencing factors in more complex modeling frameworks.

Table 4.3. ANOVA test results

Grouping Variable	F-statistic	p-value	Interpretation
TC	1.625	0.221806	Not significant
UCS	2.199	0.137022	Not significant
CAI	5.47	0.012738	Significant
Alpha	5.009	0.017232	Significant
CP	9.737	0.001115	Significant

To complement the ANOVA results, boxplot visualizations were generated for each parameter using the defined groupings (Low, Medium, High). These plots work as an intuitive graphical tool to illustrate how the dependent variable, ROP, is distributed across the categorical groups of each parameter. In a boxplot, the central line represents the median, the box shows the interquartile range (IQR) from Q1 to Q3, and the "whiskers" extend to the minimum and maximum values within 1.5 times the IQR (Hubert & Vandervieren, 2007). Interpreting these visualizations involves assessing both the relative position and overlap of the boxes across categories. When the boxes of different groups (e.g., Low vs. High) are well-separated with minimal overlap, this visually supports the presence of statistically significant group differences, often aligning with low p-values in ANOVA.

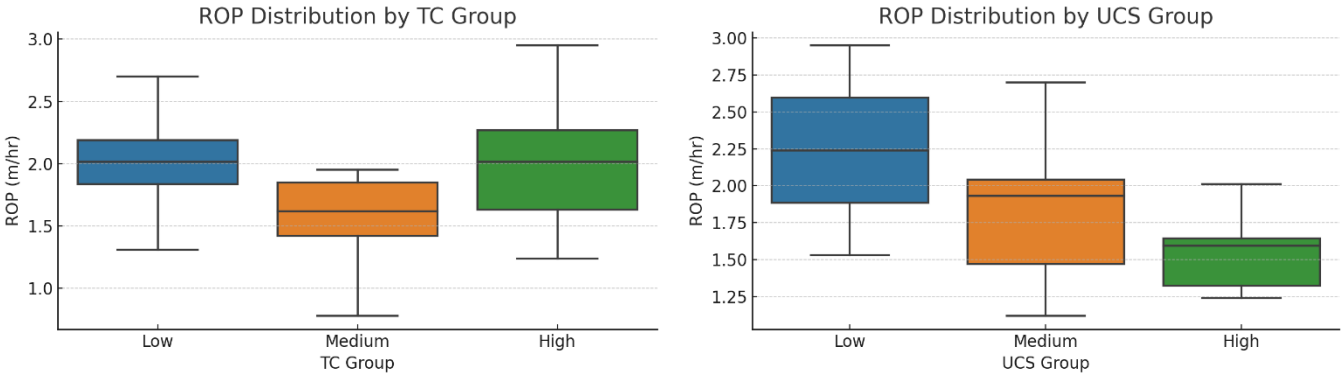

Figure 4.1. ANOVA visualizations for TC and UCS

Figure 4.1 presents the distribution of ROP across different groups of Texture Coefficient and Uniaxial Compressive Strength. Although there are visible variations between the low, medium, and high groups, the differences were not statistically significant based on ANOVA results, as mentioned earlier. For TC, the overlap in interquartile ranges across the groups suggests that variations in textural properties alone may not strongly influence TBM penetration rates within the rock types investigated. Similarly, UCS grouping shows a general trend of decreasing ROP

with increasing strength; however, the spread within each group remains wide, limiting the ability to draw strong conclusions regarding UCS as a primary control on TBM performance in this dataset.

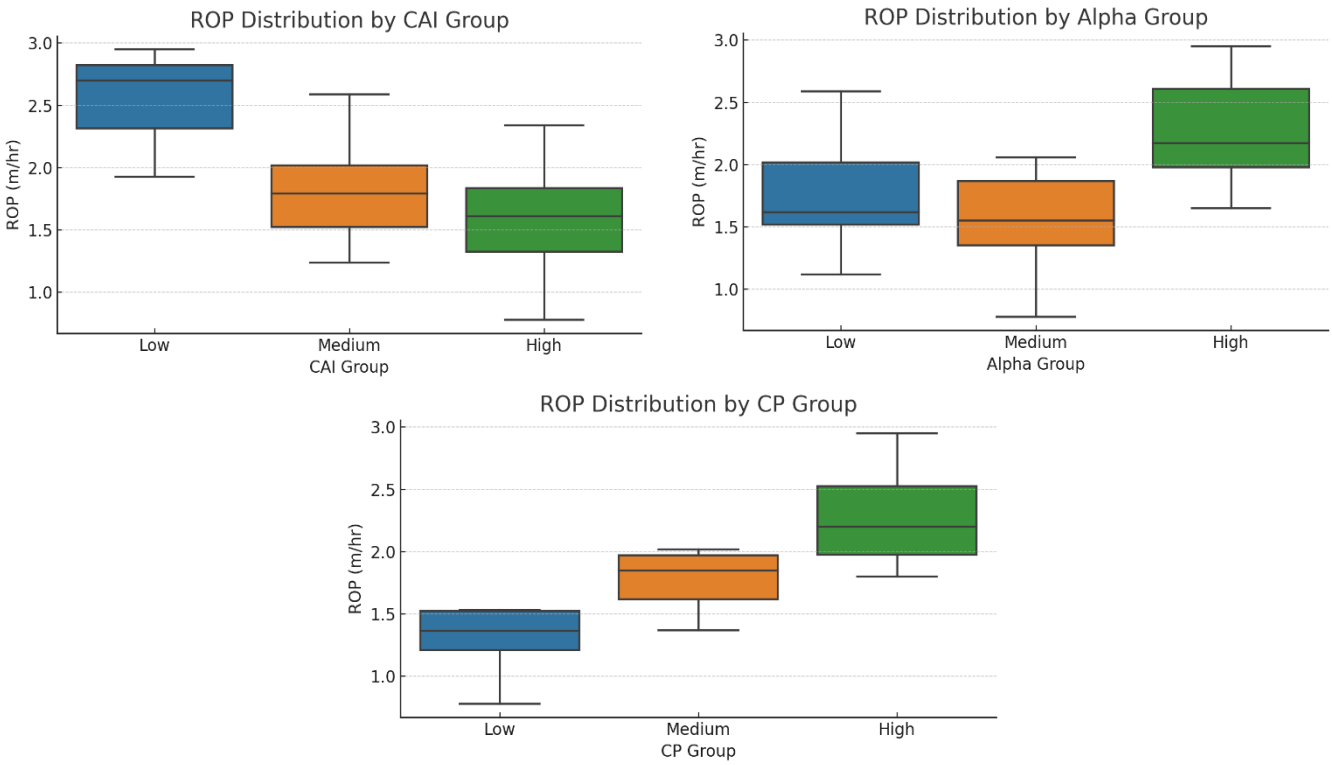

Figure 4.2. ANOVA visualizations for CAI, Alpha Angle, and CP

In contrast, the distributions of ROP grouped by Cerchar Abrasivity Index, Alpha Angle, and Cutterhead Power show statistically significant differences. CAI grouping reveals a clear decline in ROP with increasing abrasivity, consistent with greater cutter wear and energy loss in highly abrasive conditions. For Alpha Angle, higher values are associated with greater ROPs, indicating that joint orientation favorably influences fragmentation and TBM advance rates. Cutterhead Power grouping displays a strong positive relationship with ROP, with higher power inputs corresponding to higher penetration rates, reflecting the capability of the TBM to overcome rock resistance. These findings highlight that both rock mass characteristics and machine operation parameters play critical roles in determining TBM performance.

4.3. Simple Regression

Since the ultimate objective of this study is to develop a predictive model for the TBM's advance rate in hard rock environments, particularly within metamorphic formations, ROP is treated as the dependent variable in all statistical analyses. As the initial step of a regression study, it is essential to examine the individual relationships between ROP and the available parameters to identify those with the strongest correlations for inclusion in the final predictive model. This simple regression analysis was conducted using the 'Curve Estimation' function in SPSS, which determines both the strength and nature of the relationship between each independent parameter and ROP. The equations used for this procedure among the five basic models (linear, logarithmic, inverse, power, and exponential) are given in Table 4.4.

Table 4.4. Simple regression model equations

Model	Equation
Linear	$Y = b_0 + b_1 * x$
Logarithmic	$Y = b_0 + b_1 * \ln(x)$
Inverse	$Y = b_0 + b_1 / x$
Power	$Y = b_0 * {b_1}^x$
Exponential	$Y = b_0 * e^{b_1 * x}$

The relationship between TC and ROP was investigated first, testing five previously mentioned regression models. As shown in Table 4.5, all models produced very low R^2 values, with the highest being 0.03 for the exponential model. This result suggests that only about 3% of the variance in ROP can be explained by TC. Furthermore, none of the models achieved statistical significance, with p-values all above 0.4, indicating a lack of strong correlation between the variables.

Table 4.5. Model summary and parameter estimates for ROP and TC correlation

Model	R^2	F	P-value	b_0	b_1
Linear	0.023	0.504	0.486	0.581	0.867
Logarithmic	0.015	0.330	0.572	1.447	0.750
Inverse	0.009	0.187	0.670	2.357	-0.891
Power	0.022	0.463	0.504	1.354	0.517
Exponential	0.030	0.640	0.433	0.937	0.381

The scatterplot of the observed data points confirms these findings (Figure 4.3). Although all regression curves show a slight positive trend, the data points are widely scattered with no clear or strong pattern aligning with any of the fitted models. This weak and statistically insignificant correlation implies that TC, when considered as a single independent variable, does not serve as a reliable predictor of ROP in the studied conditions. Nevertheless, for this research, it will be tested as a component of the final model to assess the applicability of TC for TBM performance prediction.

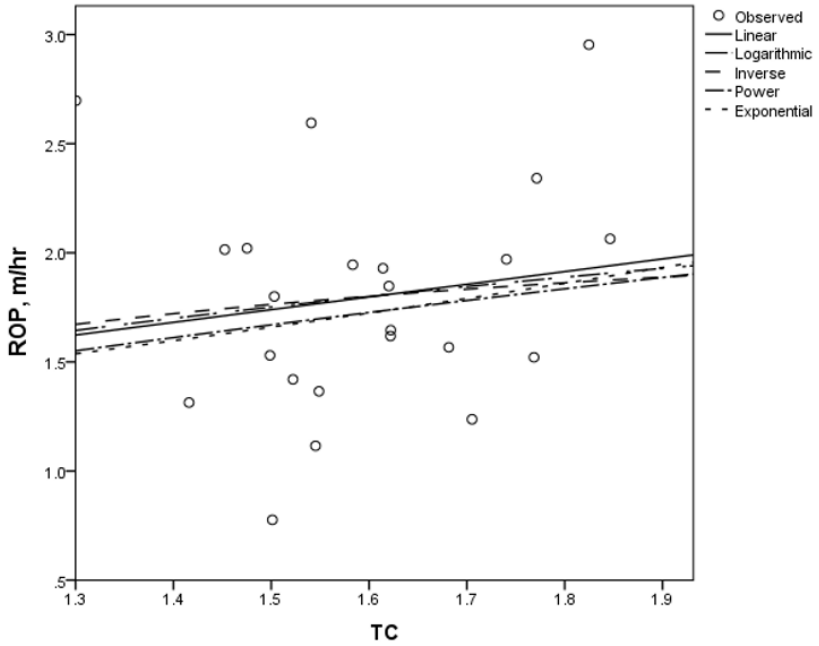

Figure 4.3. Relationship between ROP and TC

The mineralogical composition was also considered as one of the factors, potentially influencing the TBM performance in the studied project. While the potential strength-degrading feldspar presence in the available rock samples is limited to only a few specimens, the highly abrasive quartz and garnet are both found relatively frequently, allowing the performance of an analysis. However, no significant correlation was found between the mentioned minerals and the ROP (Tables 4.6-4.7; Figure 4.4). This is likely due to the indirect nature of the effect of abrasive minerals on the machine's advance rate, particularly impacting the tool wear more than the crushing and fragmentation processes. The rock mineralogy, therefore, will not be used at the later stages of regression analysis.

Table 4.6. Model summary and parameter estimates for ROP and Quartz Content correlation

	R^2	F	P-value	b_0	b_1
Linear	0.023	0.504	0.486	0.581	0.867
Logarithmic	0.015	0.330	0.572	1.447	0.750
Inverse	0.009	0.187	0.670	2.357	-0.891
Power	0.022	0.463	0.504	1.354	0.517
Exponential	0.030	0.640	0.433	0.937	0.381

Table 4.7. Model summary and parameter estimates for ROP and Garnet Content correlation

	R^2	F	P-value	b_0	b_1
Linear	0.001	0.009	0.924	1.776	-0.002
Logarithmic	0.013	0.231	0.637	1.919	-0.072
Inverse	0.042	0.795	0.384	1.656	0.674
Power	0.020	0.375	0.548	1.904	-0.054
Exponential	0.003	0.052	0.822	1.730	-0.002

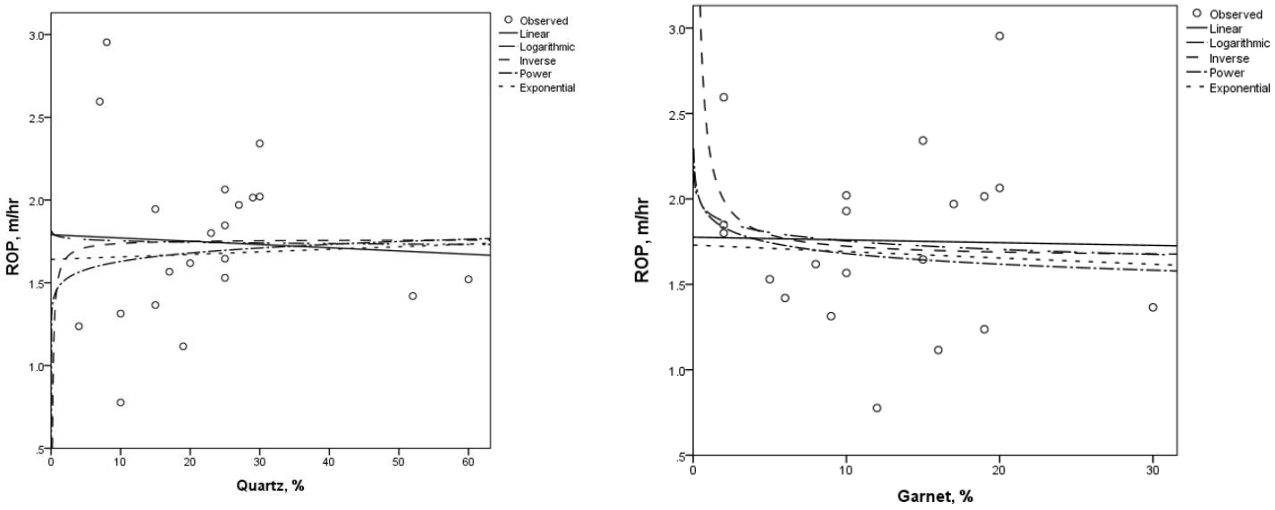

Figure 4.4. Relationship between Quartz and Garnet Content and ROP

UCS is widely used in empirical models for estimating excavation efficiency. In the present dataset, UCS exhibited a statistically significant relationship with ROP, although remaining modest. Among the tested models, the linear regression achieved the highest significance ($p = 0.046$) and an R^2 value of 0.177, indicating a weak but meaningful negative correlation (Table 4.8). The scatterplot in Figure 4.5 confirms a general downward trend between UCS and ROP, consistent with the expected behavior where higher rock strength leads to reduced penetration rates. Although the predictive strength remains moderate, the statistical significance justifies using UCS as the input for subsequent model development.

Table 4.8. Model summary and parameter estimates for ROP and UCS correlation

	R^2	F	P-value	b_0	b_1
Linear	0.177	4.509	0.046	2.809	-0.008
Logarithmic	0.162	4.060	0.057	5.949	-0.855
Inverse	0.130	3.142	0.091	1.141	81.688
Power	0.133	3.211	0.088	15.454	-0.452
Exponential	0.146	3.578	0.072	2.945	-0.004

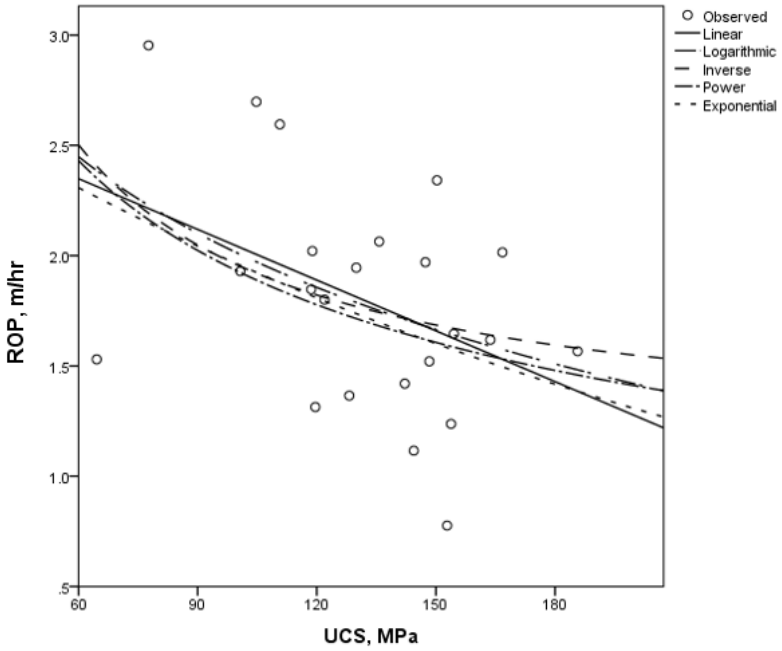

Figure 4.5. Relationship between ROP and UCS

Among all the physical and mechanical properties examined, CAI demonstrated the strongest individual correlation with ROP, achieving the highest R^2 value of 0.296 in the linear model (Table 4.9). The p-values are either below 0.01 or approaching this level for all the models, demonstrating high statistical significance. The negative slope across all models indicates a consistent inverse relationship between CAI and ROP, as higher abrasivity tends to reduce penetration rate. This trend is visually supported by the scatterplot, where the fitted curves show a clear downward trajectory (Figure 4.3). These findings align well with known TBM behavior, where more abrasive rocks typically increase cutter wear and reduce efficiency. CAI demonstrated a statistically significant relationship with ROP, confirming its potential as a meaningful predictor, especially within multivariable models in combination with other parameters.

Table 4.9. Model summary and parameter estimates for ROP and CAI correlation

	R^2	F	P-value	b_0	b_1
Linear	0.296	8.811	0.007	3.946	-0.484
Logarithmic	0.284	8.316	0.009	4.622	-1.906
Inverse	0.267	7.662	0.012	0.130	7.255
Power	0.240	6.638	0.018	7.860	-1.024
Exponential	0.253	7.122	0.014	5.504	-0.261

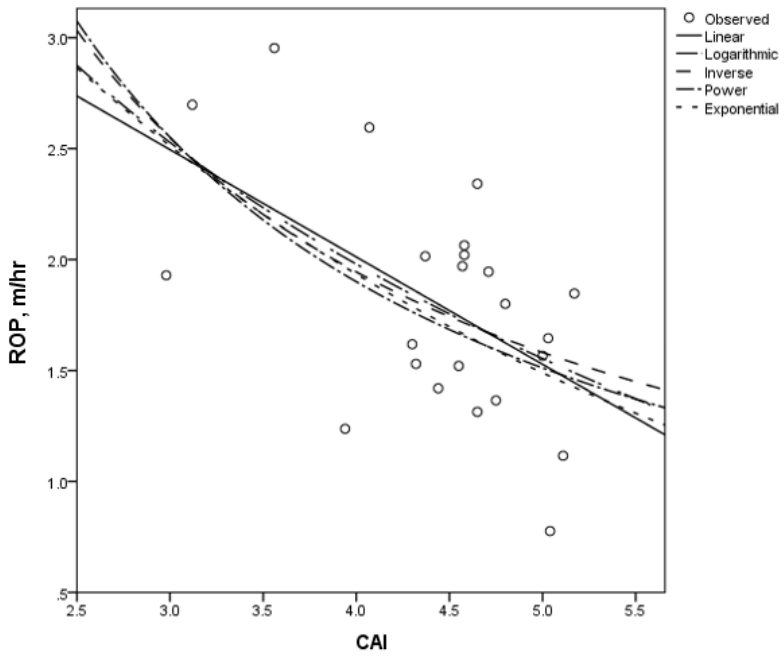

Figure 4.6. Relationship between ROP and CAI

The remaining physical properties, namely, BTS, BI, Mohs hardness, and density, lacked any statistically important correlation with ROP and were, therefore, excluded from the model development.

Among the machine parameters tested, both cutterhead power and cutterhead torque showed strong and statistically significant correlations with ROP. The highest R^2 values were 0.677 for torque and 0.650 for power, with all models yielding p-values below 0.001, indicating highly significant relationships (Table 4.10). While torque had a slightly stronger statistical fit, cutterhead power is more practical and intuitive for use in predictive modeling, as it is a more directly monitored and reported parameter in tunneling operations. The positive slopes across all models confirm a strong, direct relationship, as higher cutterhead power leads to an increased advance rate. This is clearly illustrated in the scatterplot, where the fitted curves closely follow the upward trend of the data points (Figure 4.7). These results support the selection of cutterhead power as a primary input in the final predictive model. Its high explanatory power and operational relevance make it a reliable and interpretable variable for estimating TBM performance.

Table 4.10. Model summary and parameter estimates for ROP and CP correlation

	R^2	F	P-value	b_0	b_1
Linear	0.649	38.822	0.000	2.257	0.00003
Logarithmic	0.607	32.483	0.000	-8.567	1.501
Inverse	0.553	26.012	0.000	3.125	-1277.555
Power	0.628	35.510	0.000	0.004	0.891
Exponential	0.650	39.006	0.000	0.644	0.001

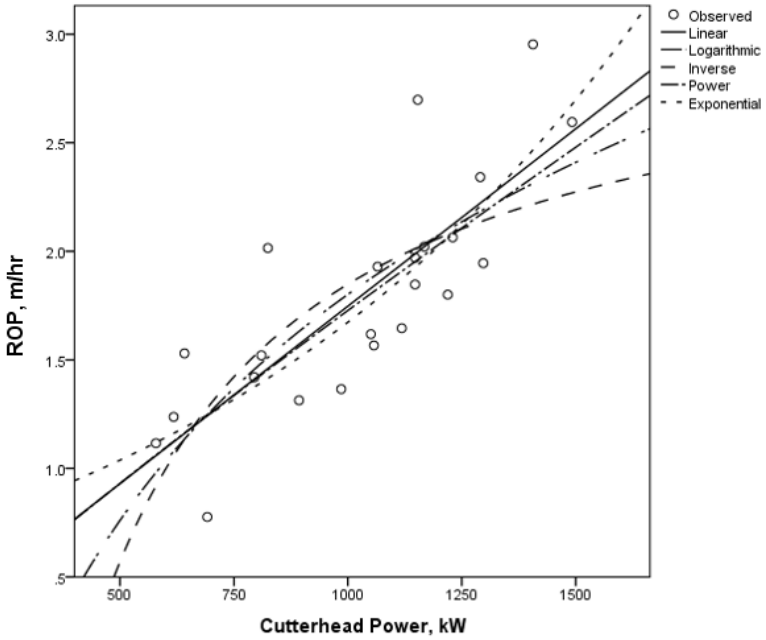

Figure 4.7. Relationship between ROP and CP

Despite being directly responsible for the TBM movement and rock-machine interaction, thrust did not show any correlation with ROP in the obtained dataset and, as such, was not considered for developing the predictive models. A possible explanation for this phenomenon lies in the relatively consistent and controlled thrust values applied during the Queens Water Tunnel excavation project. Since thrust was generally maintained within an operationally optimized range to avoid equipment overload or rock mass damage, it did not vary enough across the dataset to reveal a meaningful relationship with ROP.

Additionally, at a later stage of the regression analysis, it was decided to utilize the Alpha Angle parameter to improve the predictive power of the models and to incorporate the rock mass property feature in the equation. While not statistically significant by itself, reaching 16.8% R^2 at maximum with a linear equation (Table 4.11), this parameter is still comparably viable within the provided dataset, being the second after CAI among the physical and rock mass properties in terms of its initial fit to the ROP, which is confirmed by a relationship graph (Figure 4.8), displaying a slightly positive trend. The remaining correlation model tables and scatterplots not included in this chapter are presented in Appendix B.

Table 4.11. Model summary and parameter estimates for ROP and Alpha Angle correlation

	R^2	F	P-value	b_0	b_1
Linear	0.168	3.228	0.091	1.258	0.012
Logarithmic	0.088	1.551	0.231	0.577	0.331
Inverse	0.033	0.539	0.473	1.952	-5.637
Power	0.058	0.985	0.336	0.958	0.156
Exponential	0.128	2.352	0.145	1.296	0.006

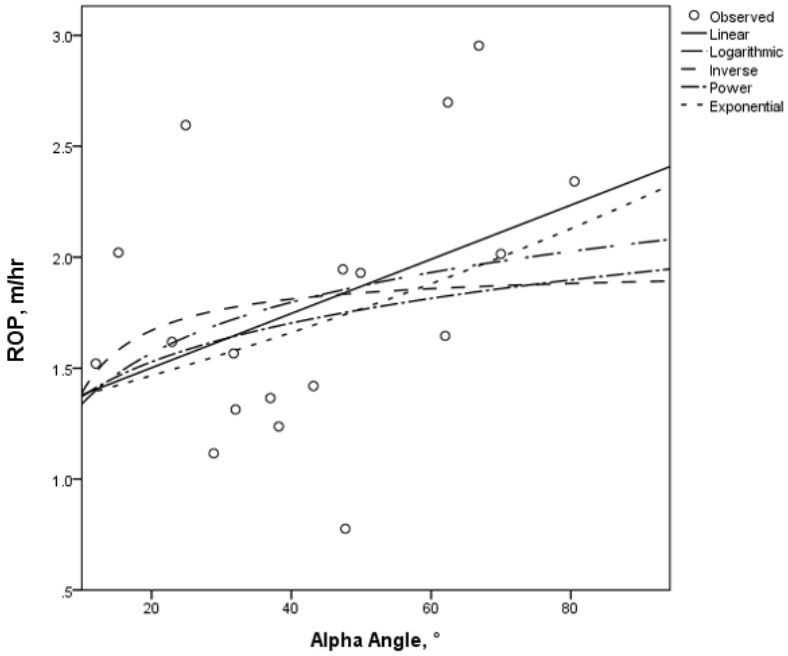

Figure 4.8. Relationship between ROP and Alpha Angle

4.4. Linear Multivariable Regression Results

Following the preliminary statistical analyses, multivariable linear regression modeling was performed to assess the combined effect of rock and machine parameters on ROP. The input variables considered were TC, UCS, CAI, α, and CP based on the previously performed analytical steps, which revealed the promising ROP predictors.

First, to understand further the relationship between the dependent and independent variables, as well as to assess the internal relationships among the independent variables, the Pearson correlation matrix was created (Table 4.12). The Pearson correlation (r) measures the strength and direction (positive or negative) of a linear relationship between two variables (James et al., 2017). The matrix revealed that CP exhibited the strongest positive correlation with ROP ($r = 0.806$, $p < 0.01$), followed by a moderate negative correlation between ROP and CAI ($r = -0.544$,

$p < 0.01$) and ROP and UCS ($r = -0.420$, $p < 0.05$). TC and Alpha Angle showed weaker correlations with ROP, suggesting that these factors individually had limited influence when not considered together with other variables. It is also notable that UCS and CAI demonstrated a moderate positive correlation ($r = 0.491$, $p < 0.05$), although the nature of these parameters, strength and abrasivity, does not necessarily imply any connection. Nevertheless, this instance required further attention during multicollinearity checks to ensure that the combined effect of these predictors would not distort the regression modeling.

Table 4.12. Pearson correlation matrix

Variable	ROP	TC	UCS	α	CAI	CP
ROP	1	0.153	-0.420*	0.410	-0.544**	0.806**
TC	0.153	1	0.193	0.056	0.079	0.247
UCS	-0.420*	0.193	1	-0.112	0.491*	-0.223
α	0.410	0.056	-0.112	1	-0.243	0.239
CAI	-0.544**	0.079	0.491*	-0.243	1	-0.186
CP	0.806**	0.247	-0.223	0.239	-0.186	1

* Correlation is significant at the 0.05 level.
** Correlation is significant at the 0.01 level.

To assess the presence of multicollinearity, Variance Inflation Factor (VIF) values and Tolerance scores were examined for each predictor (Table 4.13). VIF measures how much the variance of a regression coefficient is inflated due to multicollinearity with other predictors and is calculated from the correlation of a given variable with all the other predictors (James et al., 2017). Lower VIF values indicate minimal collinearity, with values below 5 or 10 generally considered acceptable, and values below 2.5 preferred for more conservative modeling practices. In this analysis, all VIF values were well below critical thresholds, with the highest VIF observed for UCS (2.187) and corresponding Tolerance of 0.457 (found as reciprocal of VIF). These values confirm that multicollinearity is not a concern for the dataset, and all selected variables were retained for model development.

Table 4.13. Collinearity Statistics

Predictor	Tolerance	VIF
TC	0.921	1.086
UCS	0.457	2.187
Alpha	0.891	1.122
CAI	0.551	1.816
CP	0.676	1.480

A series of multivariable regression models were developed, gradually incorporating different combinations of predictors. The comparison of model performance based on R^2, Adjusted R^2, and Standard Error showed that models including CP and CAI consistently yielded higher predictive power. The two-variable model using CAI and CP achieved an R^2 of 0.81 and an Adjusted R^2 of 0.791. Expanding the models to include additional variables slightly improved R^2 values, with the most comprehensive models (including CAI, CP, UCS, Alpha, and TC) reaching an R^2 of 0.849 and an Adjusted R^2 of 0.786, while sacrificing the model accuracy due to the increased error (0.2695 in Model 8 as opposed to 0.2381 in Model 1). Model comparison further highlighted that the inclusion of Alpha Angle slightly enhanced model performance (Adjusted R^2 = 0.817 in Model 4). However, the inclusion of TC or UCS had a minimal impact on the model's predictive strength, reflecting their weak individual correlation with ROP.

Table 4.14. Linear regression models

№	Model Components	R^2	Adjusted R^2	Std. Error
1	CAI, CP	0.81	0.791	0.2381
2	CAI, CP, UCS	0.814	0.785	0.2414
3	CAI, CP, TC	0.81	0.78	0.2443
4	CAI, CP, α	0.849	0.817	0.2496
5	CAI, CP, TC, UCS	0.815	0.773	0.2477
6	CAI, CP, TC, α	0.849	0.803	0.2589
7	CAI, CP, UCS, α	0.849	0.803	0.2591
8	All variables	0.849	0.786	0.2695

The assessment of the variables' behavior and significance within the multivariable models through Pearson correlation and p-values is shown in Table 4.15. Both CAI and CP demonstrated a substantial correlation degree and, similarly to the results shown in the Pearson matrix, had p-values generally less than 0.01. Alpha Angle proved to be a useful contributor to the models, as evident by Table 4.14; in terms of its correlation and significance, it approaches the thresholds of importance. TC and UCS, however, exhibited weak and statistically insignificant contributions in the multivariable context ($p = 0.501$ for UCS and $p = 0.839$ for TC). Their low Pearson correlation coefficients and high p-values indicate that when CP and CAI are accounted for, neither UCS nor TC substantially improves the model's predictive power. This suggests that UCS and TC are less critical factors for predicting ROP when operational machine parameters and rock abrasivity are already included.

Table 4.15. Linear regression model components

№	Model Components	CAI		CP		Alpha		TC		UCS	
		r	p	r	p	r	p	r	p	r	p
1	CAI, CP	-0.408	0.001	0.73	<0.001						
2	CAI, CP, UCS	-0.372	0.004	0.719	<0.001					-0.077	0.508
3	CAI, CP, TC	-0.409	0.001	0.728	<0.001			0.005	0.96		
4	CAI, CP, α	-0.358	0.006	0.682	<0.001	0.16	0.165				
5	CAI, CP, TC, UCS	-0.372	0.005	0.712	<0.001			0.022	0.839	-0.083	0.501
6	CAI, CP, TC, α	-0.356	0.009	0.685	<0.001	0.16	0.18	-0.012	0.911		
7	CAI, CP, UCS, α	-0.358	0.028	0.683	<0.001	0.159	0.186			0.001	0.994
8	All variables	-0.359	0.035	0.687	<0.001	0.16	0.204	-0.013	0.912	0.005	0.976

The selected regression equations for the best-performing models, Model 1 – lowest Standard Error with reasonable R^2 and Adjusted R^2 values, and Model 4 – highest R^2 and Adjusted R^2 with only a slight increase in Standard Error, as well as for Model 8, as the most comprehensive one, are presented below:

Model 1: $\text{ROP}\ (m/hr) = 1.885 - 0.363 * \text{CAI} + 0.001 * \text{CP}$

Model 4: $\text{ROP}\ (m/hr) = 1.498 - 0.331 * \text{CAI} + 0.002 * \text{CP} + 0.005 * \alpha$

Model 8: $\text{ROP}\ (m/hr) = 1.570 - 0.057 * \text{TC} + 0.001 * \text{UCS} + 0.005 * \alpha - 0.332 * \text{CAI} + 0.002 * \text{CP}$

Additionally, a stepwise linear regression was performed to automatically select the most significant predictors. The stepwise procedure retained only CAI and CP, achieving an R^2 of 0.826 and an Adjusted R^2 of 0.803 (Table 4.16). In this reduced model, CP remained a strong positive predictor ($p < 0.001$) and CAI a significant negative predictor ($p = 0.004$). The exclusion of TC, UCS, and Alpha Angle further emphasizes the limited role of textural and mechanical strength parameters in explaining ROP variability compared to operational and abrasivity factors within the dataset of this study. This model was selected as the most optimal one from the models produced by linear regression. The equation and relationship between the actual and predicted ROP by the stepwise model (Figure 4.9) are given below.

Table 4.16. Stepwise linear regression model

Model Components	R^2	Adjusted R^2	Std. Error, m/hr
CAI, CP	0.826	0.803	0.259

Table 4.17. Stepwise linear regression model components

Model Component	Coefficient	p-value
CAI	-0.358	<0.001
CP	0.002	0.004

$$\text{ROP}\ (m/hr) = 1.758 - 0.358 * \text{CAI} + 0.002 * \text{CP}$$

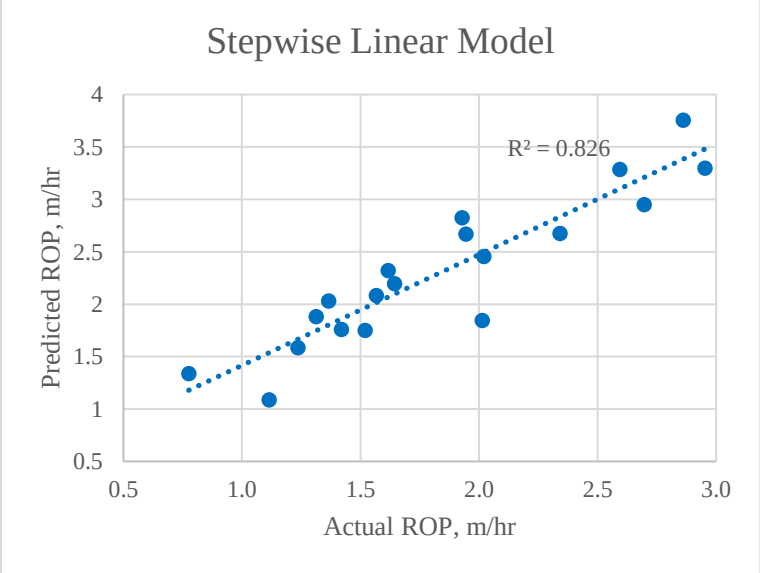

Figure 4.9. Relationship between actual and predicted ROP (Stepwise Model)

4.5. Non-linear Multivariable Regression Results

To capture the potential complex relationships between ROP and the influencing variables, a series of non-linear multivariate regression models were developed. Despite most of the data having normal distribution, as evident by histograms presented in Chapter 3, and the linear type of relationship usually displaying the best fit during the simple regression step, this attempt was made to assess any opportunities for improving the predictive model. Several equation forms were considered during the modeling process to effectively capture the non-linear interaction between the selected variables. Using the non-linear regression module in SPSS, over 30 various models were developed and tested, each incorporating a slightly different mathematical approach, including compound multiplicative power models, fractional power format, exponential functions to capture potential asymptotic behaviors, and ratio-based structure, emphasizing the opposing effects of abrasivity and rock texture against the influence of machine input. Based on this iterative process, the most optimal general form of the non-linear model equation was designed to reflect the opposing effects of positively and negatively correlated parameters on ROP and to allow for the flexible fitting of non-linear power terms:

$$ROP = c * \frac{\sum_{i=1}^{n} m_i^{p_i}}{\sum_{i=1}^{n} n_i^{p_i}}$$

where c and p_i are coefficients, m_i are the variables with positive correlation to ROP, and n_i are the variables with negative correlation to ROP.

Accordingly, three non-linear models were produced that could be directly compared to the linear models 1, 4, and 8 due to the similarity in the used variables (Table 4.18). Non-linear Model 1 implemented previously mentioned ratio-based form using only CP and CAI, yielding an R^2 of 0.798 and a standard error of 0.267 m/hr, indicating reasonable predictive capacity. Model 2 introduced α into the numerator, aiming to capture additional effects on ROP coming from the rock mass jointing orientation. This configuration produced the highest R^2 value of 0.852 and the lowest standard error (0.255) among all non-linear models. The inclusion of Alpha Angle significantly improved model fit, reflecting its positive correlation with ROP as previously observed in linear analysis. Model 3 further expanded the ratio expression by adding TC and UCS to the denominator. While this model maintained a high R^2 value of 0.816, the standard error increased to 0.298 m/hr. Notably, the exponent on CAI (15.362) became excessively high,

indicating extreme sensitivity to small variations in CAI. This suggests a risk of overfitting and numerical instability in practical applications, making the model less robust despite its theoretical appeal. Figure 4.10 demonstrates the relationship between actual and predicted by Model 2 ROP.

Table 4.18. Non-linear regression models

№	Parametric model	Fitted model	R^2	Std. Err.
1	$ROP = c * \frac{CP^{p_1}}{CAI^{p_2}}$	$ROP = 0.011 * \frac{CP^{0.874}}{CAI^{0.677}}$	0.798	0.267
2	$ROP = c * \frac{CP^{p_1} + \alpha^{p_2}}{CAI^{p_3}}$	$ROP = 0.003 * \frac{CP^{1.050} + \alpha^{1.376}}{CAI^{0.587}}$	0.852	0.255
3	$ROP = c * \frac{CP^{p_1} + \alpha^{p_2}}{CAI^{p_3} + TC^{p_4} + UCS^{p_5}}$	$ROP = 0.011 * \frac{CP^{1.043} + \alpha^{1.442}}{CAI^{-15.362} + TC^{1.588} + UCS^{0.430}}$	0.816	0.298

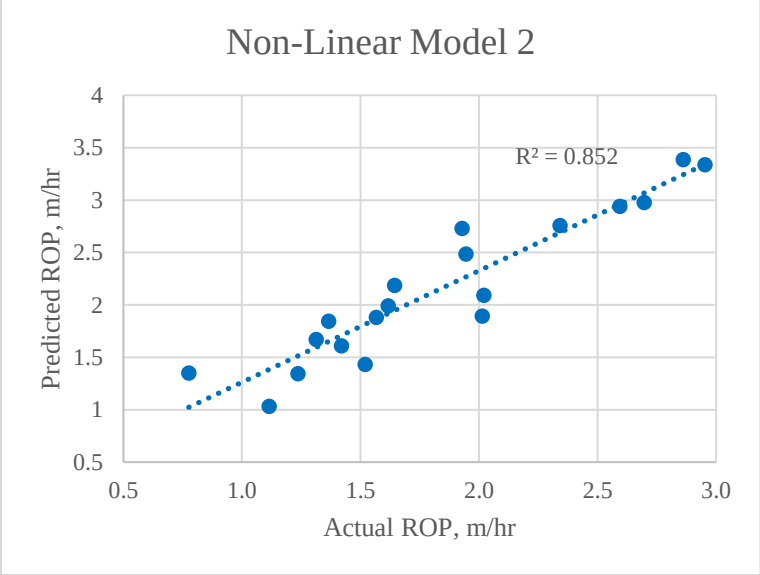

Figure 4.10. Relationship between actual and predicted ROP (Non-linear Model 2)

CHAPTER 5 – DISCUSSION

5.1. Model Selection

The regression analyses conducted in this study produced two models for estimating TBM performance under the studied geological conditions. Both the linear stepwise regression model and the non-linear regression Model 2 demonstrated high predictive capacity, with R^2 values of 0.826 and 0.852, respectively. These results indicate a strong overall correlation between the selected parameters and ROP, highlighting that a combination of operational, mechanical, and rock mass properties can reliably predict machine advance rates.

Given the model performance and practical considerations, either the stepwise linear model or the non-linear Model 2 could be selected for TBM advance rate prediction under similar geological settings, depending on the data availability and the intended application. The stepwise linear model, which incorporates only CAI and CP, offers a simple, interpretable structure that is especially advantageous when a limited number of input variables are available. On the other hand, the non-linear Model 2 includes Alpha Angle along with CAI and CP, capturing more complex interactions between geological structure and machine performance, resulting in a slightly higher predictive strength.

The non-linear Model 2 utilizes a ratio-based structure, where the sum of Alpha Angle and CP is divided by CAI raised to a fitted power. This approach effectively reflects the opposing influences of cutterhead power and geological discontinuities (which facilitate penetration) against rock abrasivity (which slows penetration due to the tool wear). Its form not only provides a significant statistical fit but also aligns with established principles of TBM operation and rock mechanics. However, the higher mathematical complexity of the non-linear model may require careful calibration when applied outside the original data range.

5.2. Impact of Parameters

Among the five variables examined for modeling TBM performance, cutterhead power emerged as the most dominant and reliable predictor of ROP. As detailed in Chapter 4.3, CP demonstrated the highest individual correlation with ROP ($r = 0.806$, $p < 0.001$) and achieved R^2 values exceeding 0.65 across all tested regression forms. The ANOVA test further confirmed CP's significant impact ($p = 0.0011$), aligning higher machine power readings to the increase in ROP.

This strong dependency is in line with the mechanical principles of TBM operation, where higher cutterhead power directly translates into increased energy input available for rock fragmentation and penetration (Bilgin et al., 2016). CP, therefore, not only captures the machine's capacity to overcome rock resistance but also remains the primary driver of advance rate variability in hard rock environments.

CAI also proved to be a significant predictor of ROP. Both the simple linear regression ($r = –0.544$, $p < 0.01$) and ANOVA results ($p = 0.0127$) confirmed its negative and statistically significant correlation with penetration performance. Higher CAI values are associated with reduced ROP, a trend that is consistent with the understanding that increased rock abrasivity leads to greater cutter wear, energy loss, and more frequent maintenance interventions (Sun et al., 2023). Although the individual R^2 values for CAI were moderate (~0.30), its inclusion notably improved the model structure by accounting for cutter wear effects on TBM progress, a key operational factor often observed in metamorphic formations rich in abrasive minerals like quartz and garnet.

UCS, while conventionally regarded as a critical mechanical property in excavation studies, demonstrated only a weak and statistically borderline relationship with ROP within this research. In the simple regression analysis, UCS achieved a somewhat modest negative correlation ($r = –0.420$, $p < 0.05$) with an R^2 of 0.177 (Chapter 4.3). Although this relationship was statistically significant at the 5% level, the strength of the correlation remained low. Moreover, the ANOVA test did not confirm a significant difference in mean ROP values across UCS groups ($p = 0.1370$). In the multivariable regression models, UCS showed consistently high p-values (>0.5), indicating that it did not contribute meaningfully once CP and CAI were accounted for. Under the conditions and geological characteristics of this study, UCS alone does not significantly impact TBM advance rates, and its predictive utility appears limited.

TC, a core aspect of the study, similarly showed a very weak relationship with ROP. The simple regression yielded very low R^2 values (maximum 0.03) and non-significant p-values (>0.4), indicating no meaningful direct correlation. ANOVA results also showed no statistically significant differences between TC groups ($p = 0.2218$). Furthermore, in the multivariable regression models, TC had a negligible effect, with p-values around 0.84–0.91 and no improvement in overall model fit. These findings suggest that, in its current form, based on petrographic thin-section analysis, TC cannot be reliably applied as a predictor for ROP under the

studied conditions of metamorphic rocks. Although TC theoretically captures aspects of rock fabric and texture heterogeneity (Howarth and Rowlands, 1987), its two-dimensional, localized nature may fail to adequately represent the three-dimensional, variable textural controls that influence TBM cutter-rock interaction in the field.

Alpha Angle, though displaying only a moderate individual correlation with ROP ($r = 0.410$, $p = 0.091$), contributed positively to the multivariable models and reached statistical significance in the ANOVA test ($p = 0.0172$). Its role as an indicator of the orientation of planes of weakness in the rock mass explains its effect, with more favorable α, typically between 45° and 90°, facilitating easier fragmentation and promoting higher ROP (Salimi et al., 2017). In case of this analysis, Alpha Angle enhanced model robustness by incorporating structural geology factors critical to TBM tunneling performance.

5.3. Model Applicability

From a practical standpoint, both the stepwise linear model and the non-linear Model 2 developed in this study offer equations for estimating TBM advance rates in specific geological conditions. Their structures are relatively simple, relying on operational and geomechanical parameters that are commonly measured or estimated during project planning and execution. This accessibility makes the models practical for feasibility studies, performance forecasting, and operational decision-making in hard rock tunneling environments. The inclusion of operational parameters, rock abrasivity, and geological structures orientation ensures a comprehensive predictive mechanism that remains interpretable and adaptable across different rock mass conditions within the metamorphic terrains.

Nevertheless, several limitations of the developed models must be acknowledged. First, the models were calibrated on a dataset primarily consisting of hard, metamorphic rocks with high quartz and garnet content. Their direct applicability to different rock types remains unverified and would require additional analysis. Second, the models were built on a relatively small dataset, which could lead to potential overfitting of the produced model, which should, therefore, be tested on larger datasets with similar conditions. Third, while CAI, Alpha Angle, and CP can typically be monitored and updated in real time during excavation, variables like TC and UCS are static, laboratory-derived properties, which limit their applicability in certain scenarios, especially considering their insignificant impact on the models of the study.

CHAPTER 6 – CONCLUSIONS AND RECOMMENDATIONS

6.1. Conclusions

This study focused on assessing the boreability of hard metamorphic rocks by integrating petrographic texture analysis with mechanical and operational data from the TBM excavation project. A particular emphasis was placed on evaluating the Texture Coefficient and its relationship with TBM advance rates, together with other critical parameters. The key outcomes of the research are summarized below:

- The TC values were successfully computed from thin-section photomicrographs using a structured image analysis methodology, capturing variations in grain size, shape, and interlocking.
- A comprehensive dataset was developed, combining laboratory-measured mechanical properties and field-recorded TBM performance data from the Queens Water Tunnel project.
- Through systematic statistical analysis, two predictive models were identified as the most suitable for estimating TBM rate of penetration: a stepwise linear regression model using CP and CAI, and a non-linear regression model incorporating CP, CAI, and Alpha Angle. These models achieved R^2 values of 0.826 and 0.852, respectively, demonstrating strong predictive capabilities.
- CP was the dominant factor controlling ROP, followed by the significant negative effect of CAI and the positive contribution of α. In contrast, TC and UCS showed limited predictive value and did not improve model performance under the studied conditions.
- Overall, it could be concluded that in its current form, TC cannot serve as a reliable predictor for TBM advance rate in metamorphic formations. Based on the persistent significance of CAI, most likely for the case of the Queens Water Tunnel project, the abrasivity of metamorphic rocks played the most crucial role, while the effect of texture might either have been more subtle or might not have been fully captured by the classical TC measuring approach.

6.2. Recommendations and Future Work

Given the results of this study, it is recommended that predictive modeling of TBM penetration rate prioritize operational parameters such as power, rock mass features like orientation of joints, and rock abrasivity, especially when dealing with metamorphic formations. These factors demonstrated the strongest and most consistent influence on ROP and could be considered reliable inputs for future feasibility studies and performance forecasting in hard rock tunneling.

While the TC-based methodology for textural assessment was systematically applied during this research, its predictive power for ROP under the studied conditions was limited. Therefore, the integration of TC into boreability assessments should be approached carefully. Further research is needed to explore whether improvements in the texture analysis, including automated image analysis and TC calculation, modifications in the original equation introducing correction factors that account for texture variability in different rock types, or three-dimensional textural modeling, can enhance the relevance of TC for excavation performance prediction.

For future projects, it is recommended that geotechnical investigations continue to incorporate detailed rock mass characterization, particularly measuring parameters like CAI and α, early in the project lifecycle. Expanding datasets to include a wider variety of geological settings, rock types, and operational conditions would also help validate and improve the reliability of the developed models.

In addition, future studies could explore integrating additional operational factors, such as cutterhead design parameters and real-time monitoring outputs, into predictive frameworks. Incorporating machine learning approaches for multivariable analysis of larger datasets or dynamic model updating based on excavation feedback may also provide valuable outcomes and enhance TBM performance prediction models beyond traditional regression techniques.

REFERENCES

Atici, U., & Comakli, R. (2019). Evaluation of the physico-mechanical properties of plutonic rocks based on texture coefficient. *Journal of the Southern African Institute of Mining and Metallurgy, 119*(1). https://doi.org/10.17159/2411-9717/2019/v119n1a8

Azzoni, A., Bailo, F., Rondena, E., & Zaninetti, A. (1996). Assessment of Texture Coefficient for Different Rock Types and Correlation with Uniaxial Compressive Strength and Rock Weathering. *Rock Mechanics and Rock Engineering*, 29(1), 39–46.

Bayram, O., Ercelebi, S. G., Ozturk, C. A. (2011). Correlations among Textural, Mechanical, Physical Properties Based on Petrographical Classification of Some Natural Stones. *Mining Engineering Department of Istanbul Technical University, Istanbul, Turkey*.

Bilgin, N., Copur, H., & Balci, C. (2016). Effect of high strength rocks on TBM performance. 10.1002/9783433607190.ch11.

Brock, P. C., Brock, P. W. G., Merguerian, C. (2000). The Queens Tunnel Complex: A Newly Discovered Granulite Facies Fordham Orthogneiss Complex That Dominates the Subsurface of Western Queens. In *Geology Department, Hofstra University*.

Bruland, A., & Johannessen, O. (1998). Hard Rock Tunnel boring performance data and back-mapping. *PhD Dissertation at NTNU* (Vols. 6–10), Faculty of Engineering Science and Technology, Civil and Transport Engineering.

Çomaklı, R., Atıcı, Ü. (2022). Predicting compressive strength using the texture coefficient with soft computing techniques for rocks. In *Niğde Ömer Halisdemir Üniversitesi Mühendislik Bilimleri Dergisi* (pp. 1127–1137). https://doi.org/10.28948/ngmuh.1158645.

Delisio, A., Zhao, J., & Einstein, H. (2012). Analysis and prediction of TBM performance in blocky rock conditions at the Lötschberg Base Tunnel. *Tunnelling and Underground Space Technology*, 33, 131–142. https://doi.org/10.1016/j.tust.2012.06.015.

Ersoy, A., Jr., & Waller, M. D. (1995). Textural characterisation of rocks. In Department of Mineral Resources Engineering, The University of Nottingham, *Engineering Geology*, 39, 123-136.

Gehring, K. (1995). Leistungs- und Verschleißprognosen im maschinellen Tunnelbau. *XLIV. Geomechanik-Kolloquium 1995, 12. Und 13. Oktober 1995 in Salzburg/Austria: Kurzfassungen Der Vorträge, Teilnehmerverzeichnis*.

Ghosh, S. K., Niharika, B., Rao, K. U. M., & Pal, S. K. (2012). Rock Sample Characterization Based on Textural Features, Strength Properties and Signal Emission Levels under Application of Uni-axial Compressive Stress. *International Journal of Engineering Research & Technology (IJERT)*, 1–6.

Hassanpour, J., Rostami, J., & Zhao, J. (2011). A new hard rock TBM performance prediction model for project planning. *Tunnelling and Underground Space Technology*, *26*(5), 595–603. https://doi.org/10.1016/j.tust.2011.04.004.

Howarth, D. F. & Rowlands, J. C. (1987). Quantitative Assessment of Rock Texture and Correlation with Drillability and Strength Properties. In *Rock Mechanics and Rock Engineering* (Vols. 20–20, pp. 57–85). Springer-Verlag.

Hubert, M., & Vandervieren, E. (2007). An adjusted boxplot for skewed distributions. *Computational Statistics & Data Analysis*, 52(12), 5186–5201. https://doi.org/10.1016/j.csda.2007.11.008

James, G., Witten, D., Hastie, T., & Tibshirani, R. (2017). *An introduction to statistical learning* (8th ed.). Springer Science+Business Media.

Kamani, M., Ajalloeian, R. (2019). Evaluation of Engineering Properties of Some Carbonate Rocks Trough Corrected Texture Coefficient. *Geotech Geol Eng* 37, 599–614. https://doi.org/10.1007/s10706-018-0630-8

Macias, F. J. (2016). Hard Rock Tunnel Boring – Performance Predictions and Cutter Life Assessments. *PhD Dissertation, Norwegian University of Science and Technology.*

Merguerian, C. (2001). Brittle faults of the Queens Tunnel Complex, NYC Water Tunnel #3. In *Geology Department, Hofstra University*.

Merguerian, C. (1999). Techniques of TBM Tunnel Mapping - The Queens Tunnel, NYC. In *Geology Department, Hofstra University*.

Merguerian, C., & Ozdemir, L. (2003). Rock Mass Properties and Hard Rock TBM Penetration Rate Investigations, Queens Tunnel Complex, NYC Water Tunnel #3, Stage 2. In *2003 RETC Proceedings*.

Montgomery, D. C. (2013). *Design and analysis of experiments*. John Wiley & Sons, Inc.

Ozturk, C.A., & Nasuf, E. (2013). Strength classification of rock material based on textural properties. Tunnelling and Underground Space Technology, 37, 45-54.

Ozturk, C. A., Nasuf, E., & Sair Kahraman. (2014). Estimation of rock strength from quantitative assessment of rock texture. *Journal of the Southern African Institute of Mining and Metallurgy*, 114, 471-480.

Pandey, P. K., Raina, A. K., Deshmukh, S., Trivedi, R., Vajre, R., & Murthy, V. M. S. R. (2020). Influence of geology on tunnel boring machine performance – A review. Journal of Mining and Metallurgy, Section A: Mining, 56(1), 1-14. https://doi.org/10.5937/JMMA2001001P.

Phillipson, E. S. (1998). Thin Section Petrographic Analyses for Queen's Water Tunnel No.3, Stage 2. *Colorado School of Mines, Department of Mining Engineering, Earth Mechanics Institute.*

Qiu, P., & Pabst, T. (2023). Characterization of particle size segregation and heterogeneity along the slopes of a waste rock pile using image analysis. *Environmental Earth Sciences,* 82(23). https://doi.org/10.1007/s12665-023-11229-y.

Ribacchi, R., & Fazio, A. L. (2004). Influence of rock mass parameters on the performance of a TBM in a Gneissic formation (Varzo Tunnel). *Rock Mechanics and Rock Engineering*, 38(2), 105–127. https://doi.org/10.1007/s00603-004-0032-5.

Rostami, J. (1997). Development of a Force Estimation Model for Rock Fragmentation with Disc Cutters through Theoretical Modeling and Physical Measurement of Crushed Zone Pressure. *Colorado School of Mine, Department of Mining Engineering, Earth Mechanics Institute.*

Rostami, J., Ozdemir, L., & Nilson, B. (1996). Comparison Between CSM And NTH Hard Rock TBM Performance Prediction Models.

Salimi, A., Rostami, J., & Moormann, C. (2017). Evaluating the Suitability of Existing Rock Mass Classification Systems for TBM Performance Prediction by Using a Regression Tree. *Procedia Engineering*, *191*, 299–309. https://doi.org/10.1016/j.proeng.2017.05.185.

Schlicke, M., Wannenmacher, H., & Nübel, K. (2024). Advancing TBM performance: Integrating shield friction analysis and machine learning in geotechnical engineering. *Geotechnics*, 4(1), 194–208. https://doi.org/10.3390/geotechnics4010010.

Sun, J., Shang, Y., Wang, K., Wang, C., Ma, F., & Sun, C. (2023). A new prediction model for disc cutter wear based on Cerchar Abrasivity Index. *Wear*, *526–527*, 204927. https://doi.org/10.1016/j.wear.2023.204927

Suorineni, F. T., Chinnasane, D. R., & Kaiser, P. K. (2009). A Procedure for Determining Rock-Type Specific Hoek-Brown Brittle Parameter s. *Rock Mechanics and Rock Engineering*, 849–881. https://doi.org/10.1007/s00603-008-0024-y.

Tiryaki, B., & Dikmen, A. C. (2005). Effects of rock properties on specific cutting energy in linear cutting of sandstones by picks. *Rock Mechanics and Rock Engineering*, *39*(2), 89–120. https://doi.org/10.1007/s00603-005-0062-7.

Tugrul, A., Zarif, I. H., & Istanbul University, Department of Geological Engineering. (1999). Correlation of mineralogical and textural characteristics with engineering properties of selected granitic rocks from Turkey. In *Engineering Geology*, 51, 303–317.

Tumac, D., Copur, H., Balci, C., Er, S., & Avunduk, E. (2017). Investigation into the Effects of Textural Properties on Cuttability Performance of a Chisel Tool. *Rock Mechanics and Rock Engineering*, 51(4), 1227–1248. https://doi.org/10.1007/s00603-017-1376-y.

Tumac, D., Copur, H., Balci, C., Shaterpour-Mamaghani, A. (2018). Determining the effects of physical, mechanical and textural properties of metamorphic stones on a chisel tool performance. In *10th Asian Rock Mechanics Symposium (ARMS10)*.

Wegrzyn, R. S. (1997). Preliminary Machine Performance Analysis. *Colorado School of Mine, Department of Mining Engineering, Earth Mechanics Institute.*

Yagiz, S. (2009). Assessment of brittleness using rock strength and density with punch penetration test. Tunnelling and Underground Space Technology. 24. 66-74. 10.1016/j.tust.2008.04.002.

Yagiz, S. (2002). Development of rock fracture and brittleness indices to quantify the effects of rock mass features and toughness in the CSM model basic penetration for hard rock tunneling machines. *PhD Dissertation, T-5605, Colorado School of Mines, USA*. (I ed.).

APPENDIX A – THIN SECTION IMAGES

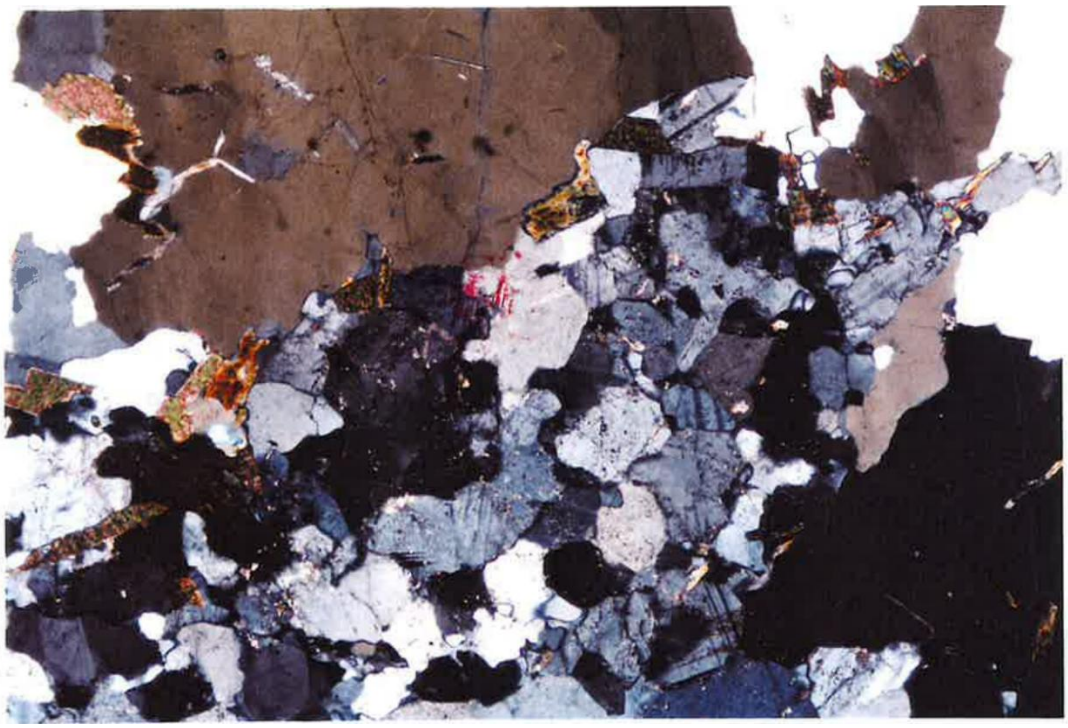

Figure 1. 1+21_a original thin section

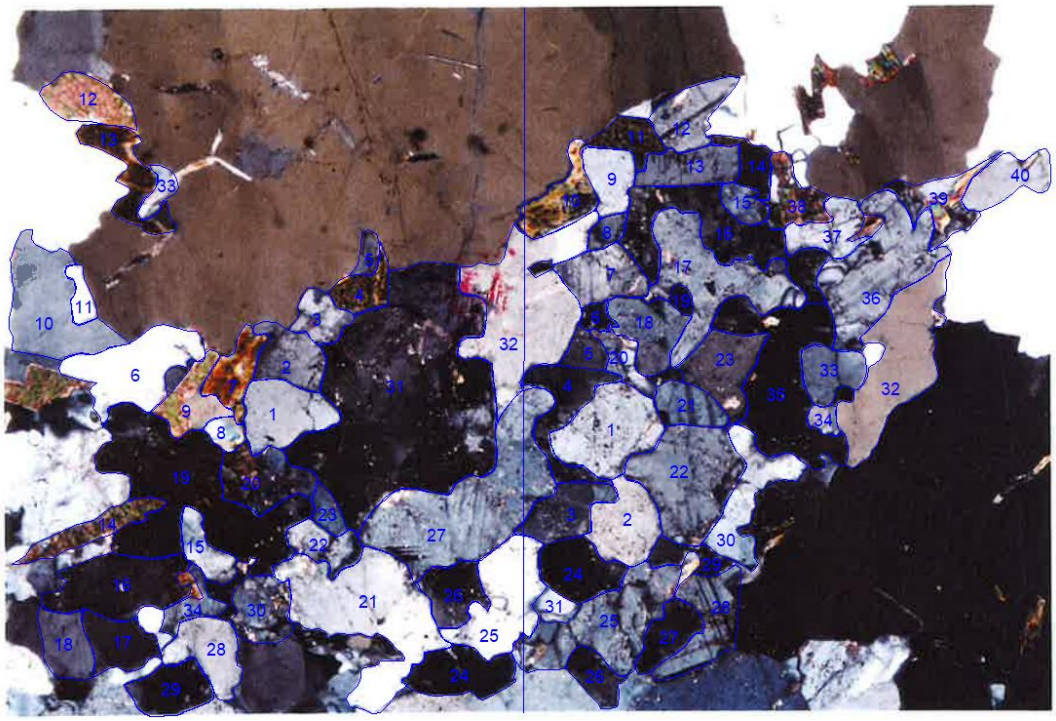

Figure 2. 1+21_a processed thin section

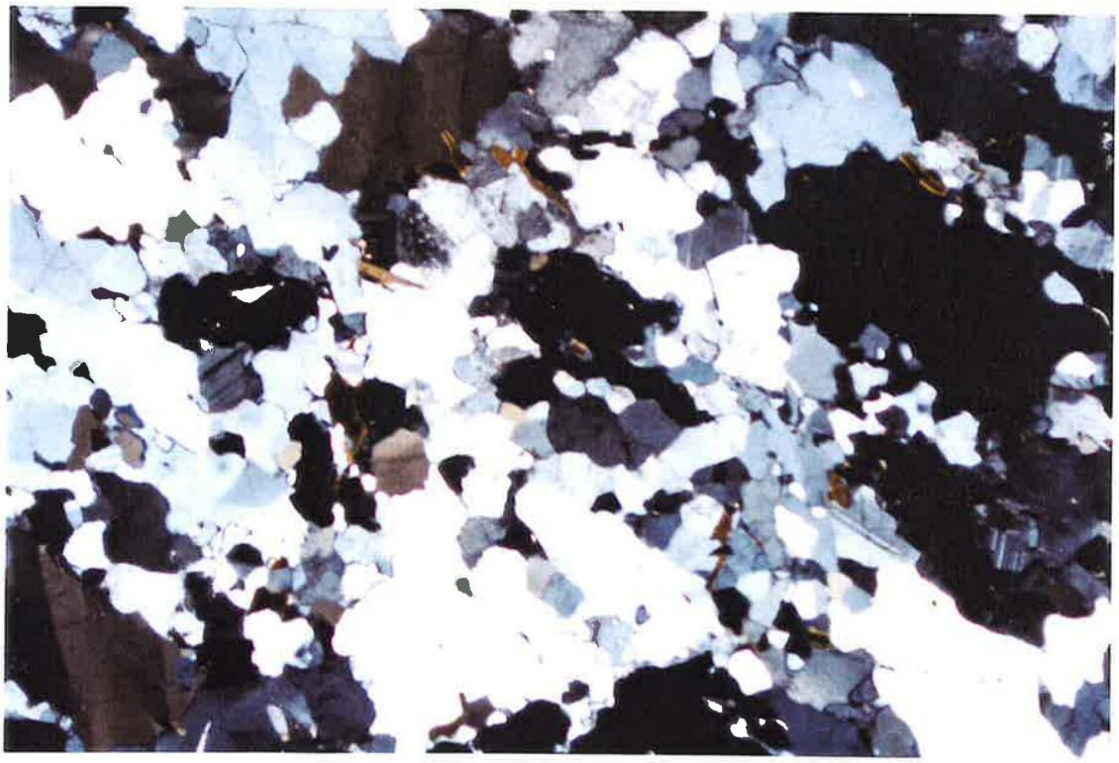

Figure 3. 1+89 original thin section

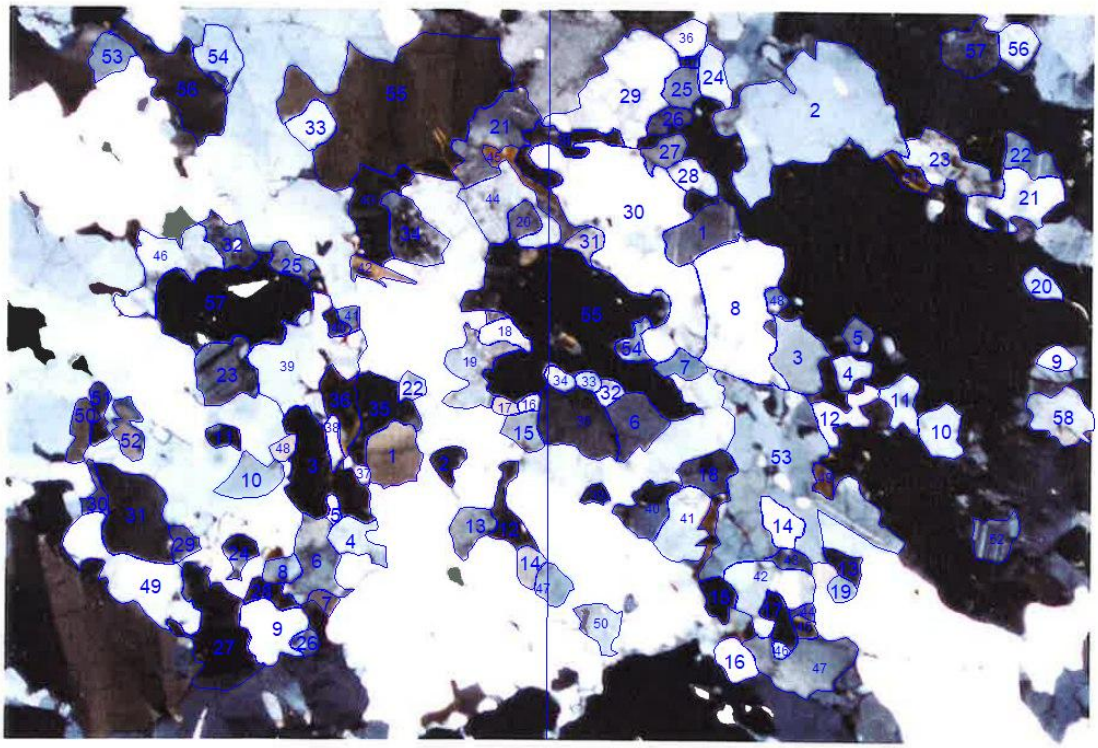

Figure 4. 1+89 processed thin section

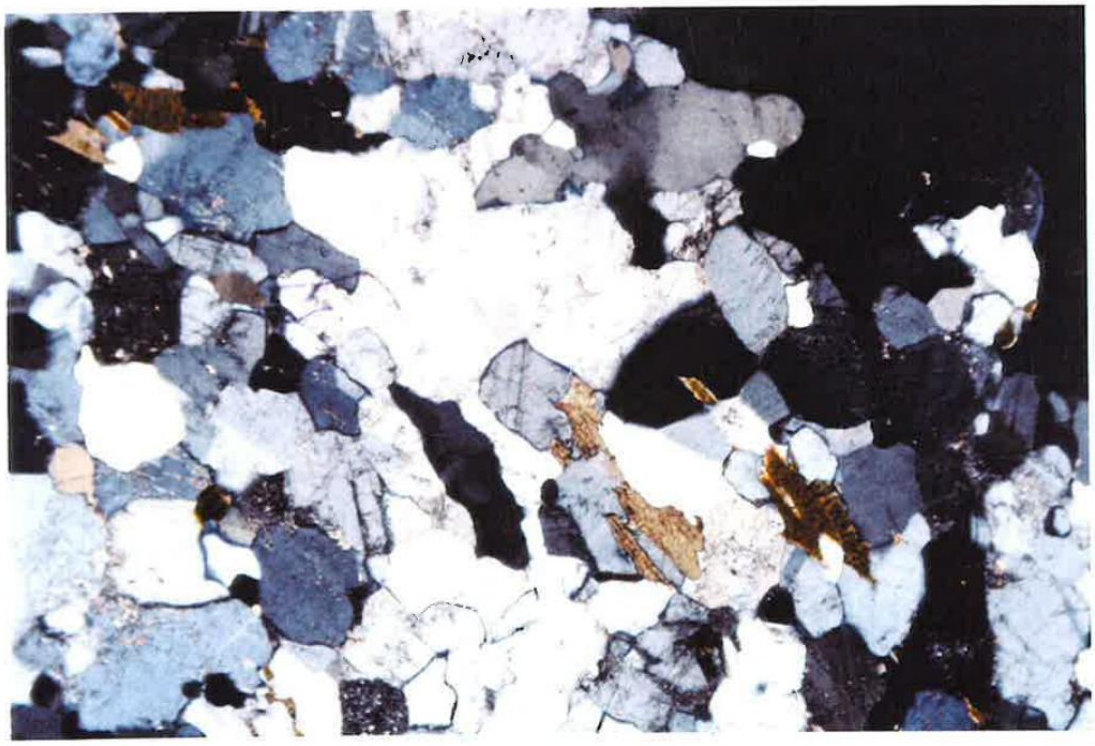

Figure 5. 1+89_a original thin section

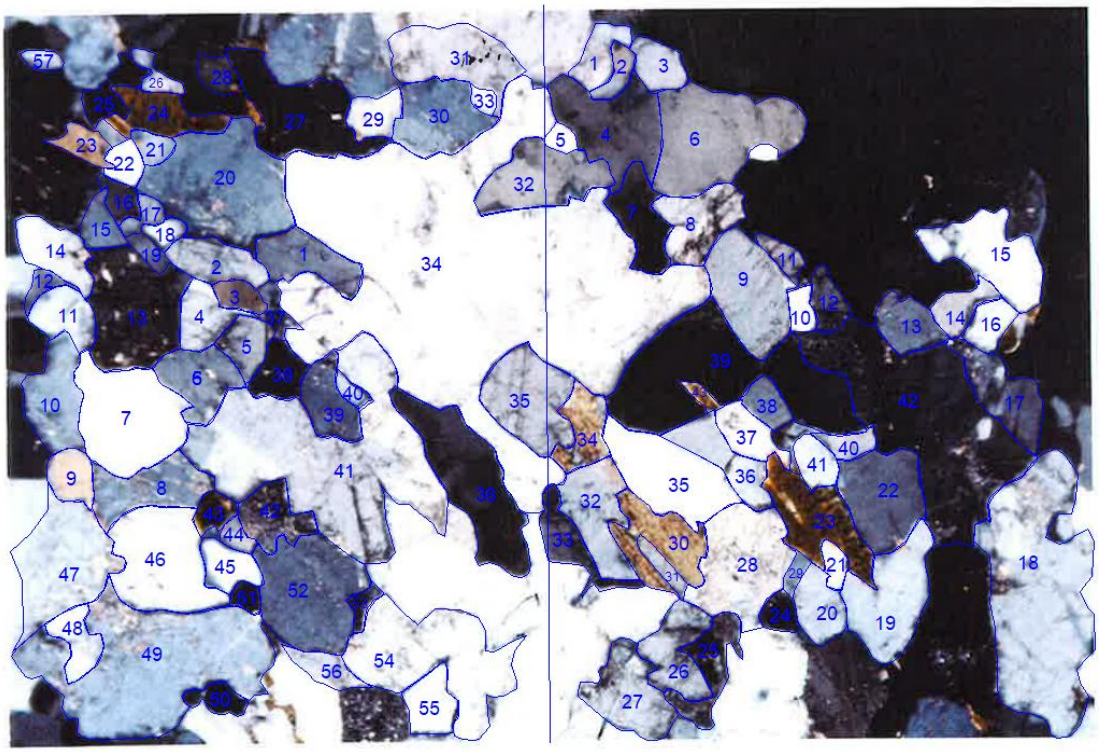

Figure 6. 1+89_a processed thin section

APPENDIX B – SIMPLE CORRELATION RESULTS

Table 1. Model summary and parameter estimates for ROP and BTS correlation

	R^2	F	P-value	b_0	b_1
Linear	0.021	0.345	0.565	1.436	0.039
Logarithmic	0.032	0.524	0.480	0.778	0.461
Inverse	0.043	0.724	0.408	2.342	-4.899
Power	0.038	0.639	0.436	0.889	0.299
Exponential	0.029	0.485	0.496	1.337	0.027

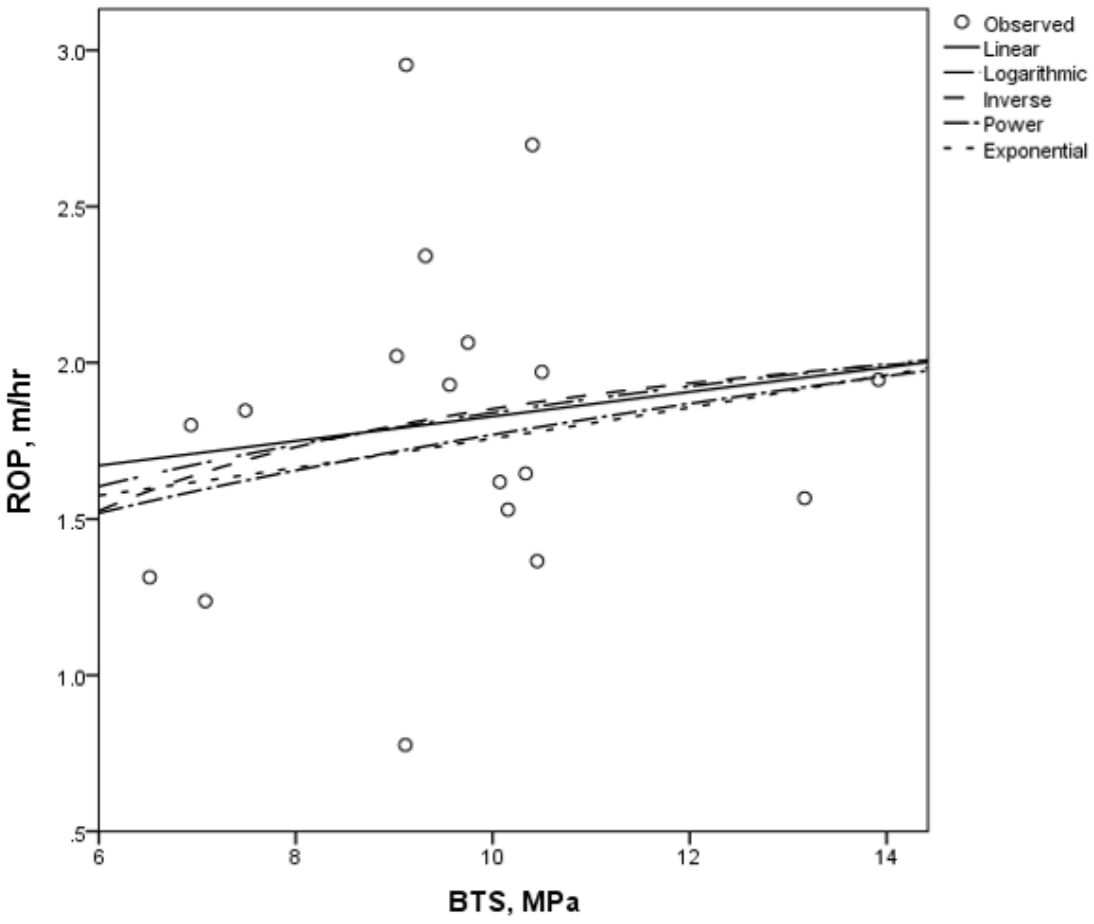

Figure 1. Relationship between ROP and BTS

Table 2. Model summary and parameter estimates for ROP and Density correlation

	R^2	F	P-value	b_0	b_1
Linear	0.007	0.149	0.704	0.868	0.328
Logarithmic	0.007	0.144	0.708	0.849	0.913
Inverse	0.007	0.139	0.713	2.695	-2.533
Power	0.000	0.000	0.990	1.752	-0.017
Exponential	0.000	0.000	0.999	1.725	-0.001

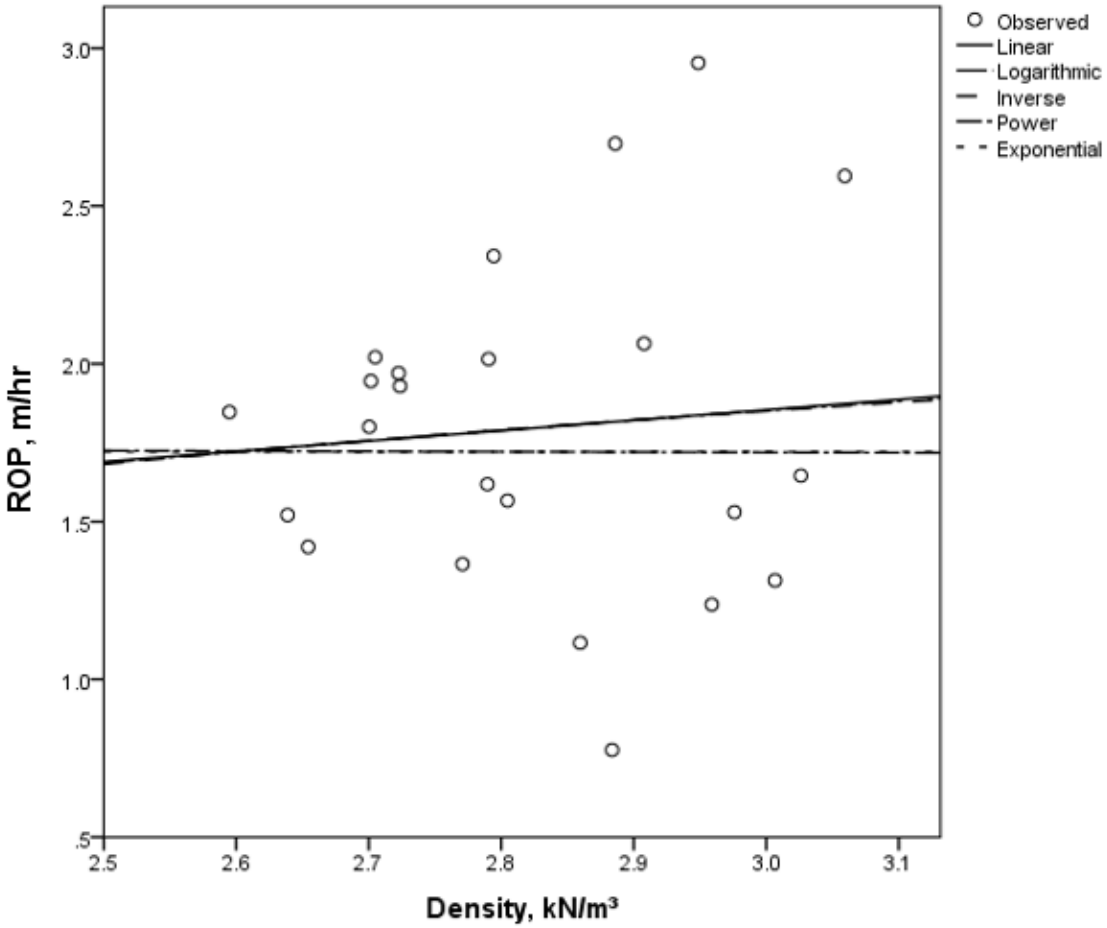

Figure 2. Relationship between ROP and Density

Table 3. Model summary and parameter estimates for ROP and BI correlation

	R^2	F	P-value	b_0	b_1
Linear	0.047	0.837	0.373	2.128	-0.007
Logarithmic	0.036	0.642	0.434	2.656	-0.223
Inverse	0.023	0.394	0.539	1.697	5.159
Power	0.050	0.896	0.357	2.987	-0.140
Exponential	0.064	1.163	0.296	2.141	-0.004

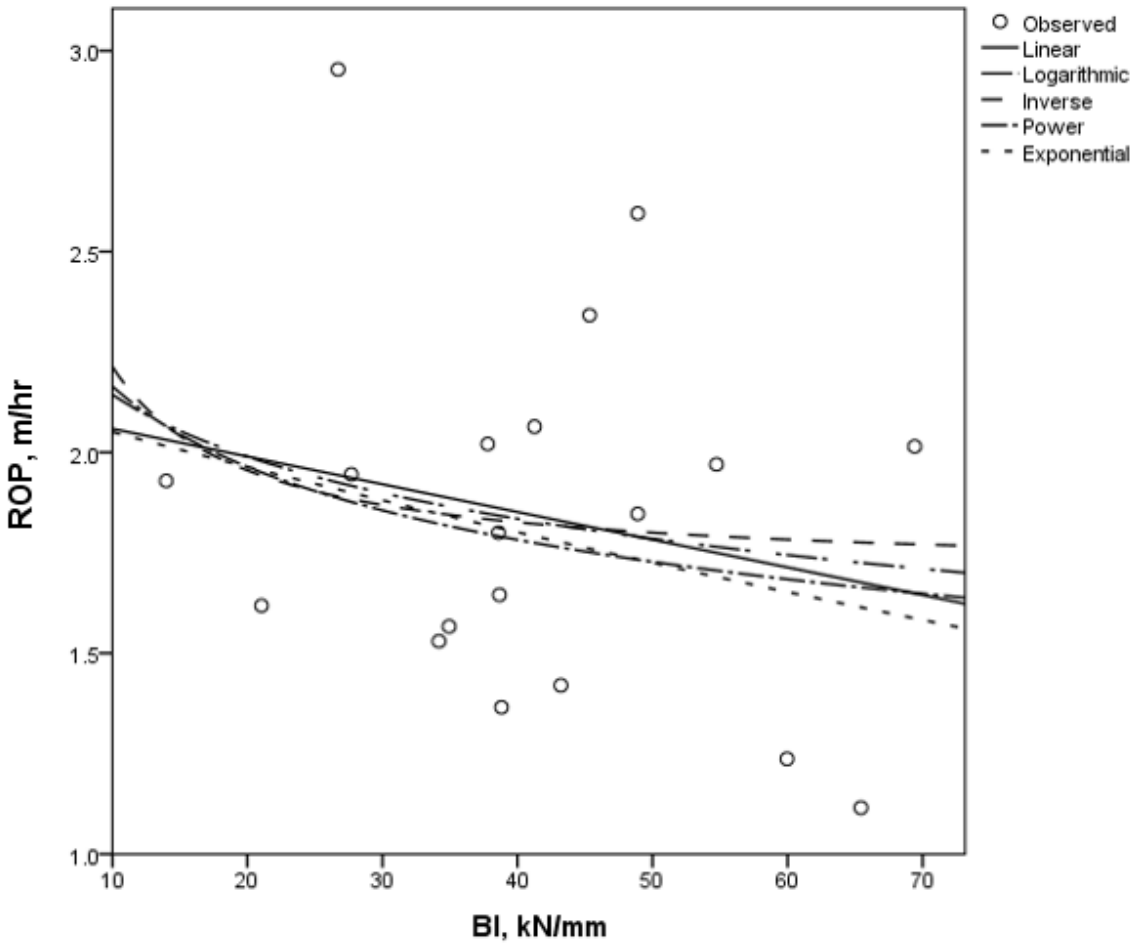

Figure 3. Relationship between ROP and BI

Table 4. Model summary and parameter estimates for ROP and Fracture Spacing correlation

	R^2	F	P-value	b_0	b_1
Linear	0.127	3.050	0.095	1.916	-0.031
Logarithmic	0.209	5.562	0.028	1.816	-0.147
Inverse	0.140	3.410	0.079	1.631	0.077
Power	0.220	5.920	0.024	1.743	-0.088
Exponential	0.156	3.892	0.062	1.861	-0.020

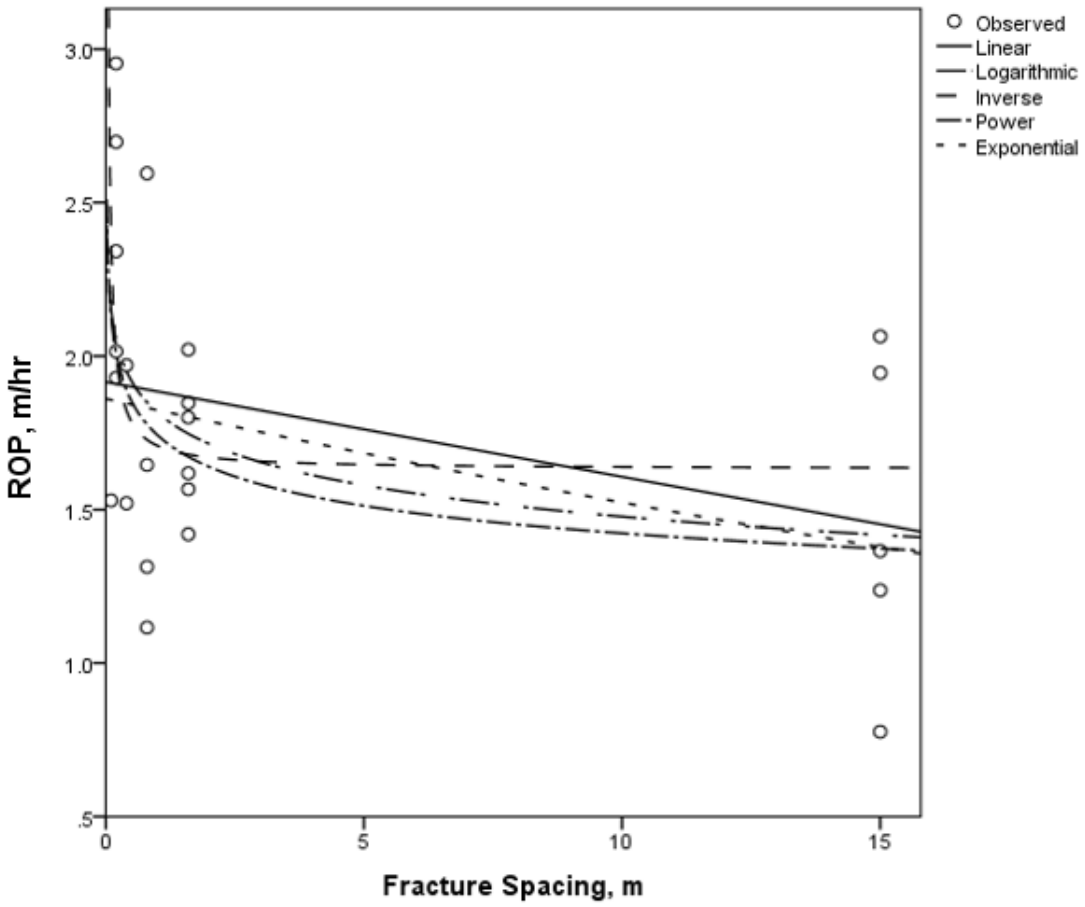

Figure 4. Relationship between ROP and Fracture Spacing

Table 5. Model summary and parameter estimates for ROP and Mohs Hardness correlation

	R^2	F	P-value	b_0	b_1
Linear	0.112	2.657	0.118	4.809	-0.498
Logarithmic	0.112	2.658	0.118	7.098	-2.949
Inverse	0.112	2.653	0.118	-1.085	17.365
Power	0.069	1.560	0.225	19.540	-1.351
Exponential	0.069	1.547	0.227	6.812	-0.227

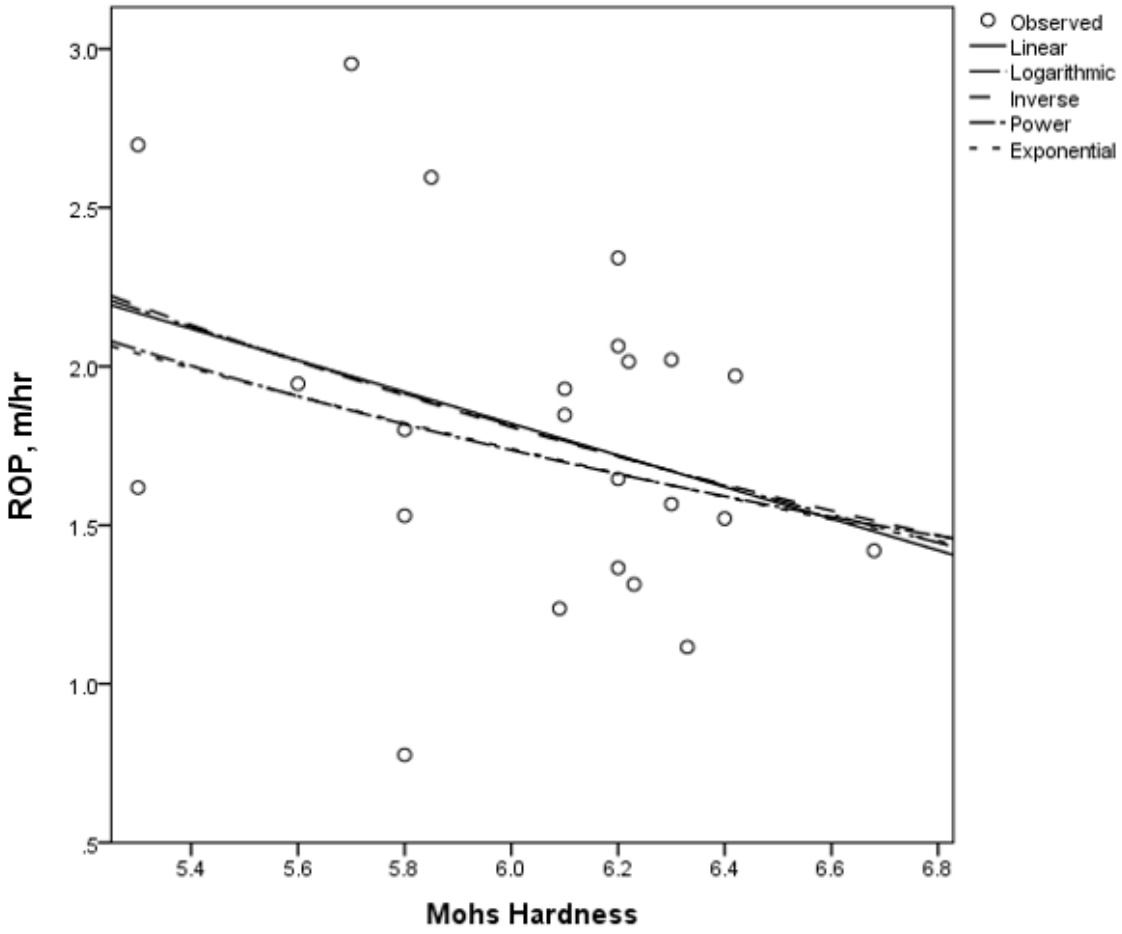

Figure 5. Relationship between ROP and Mohs Hardness

Table 6. Model summary and parameter estimates for ROP and Net Thrust correlation

	R^2	F	P-value	b_0	b_1
Linear	0.018	0.380	0.544	2.257	-3.093E-5
Logarithmic	0.012	0.257	0.617	5.123	-0.347
Inverse	0.007	0.146	0.706	1.560	3419.706
Power	0.015	0.310	0.584	14.481	-0.222
Exponential	0.019	0.413	0.528	2.279	-1.880E-5

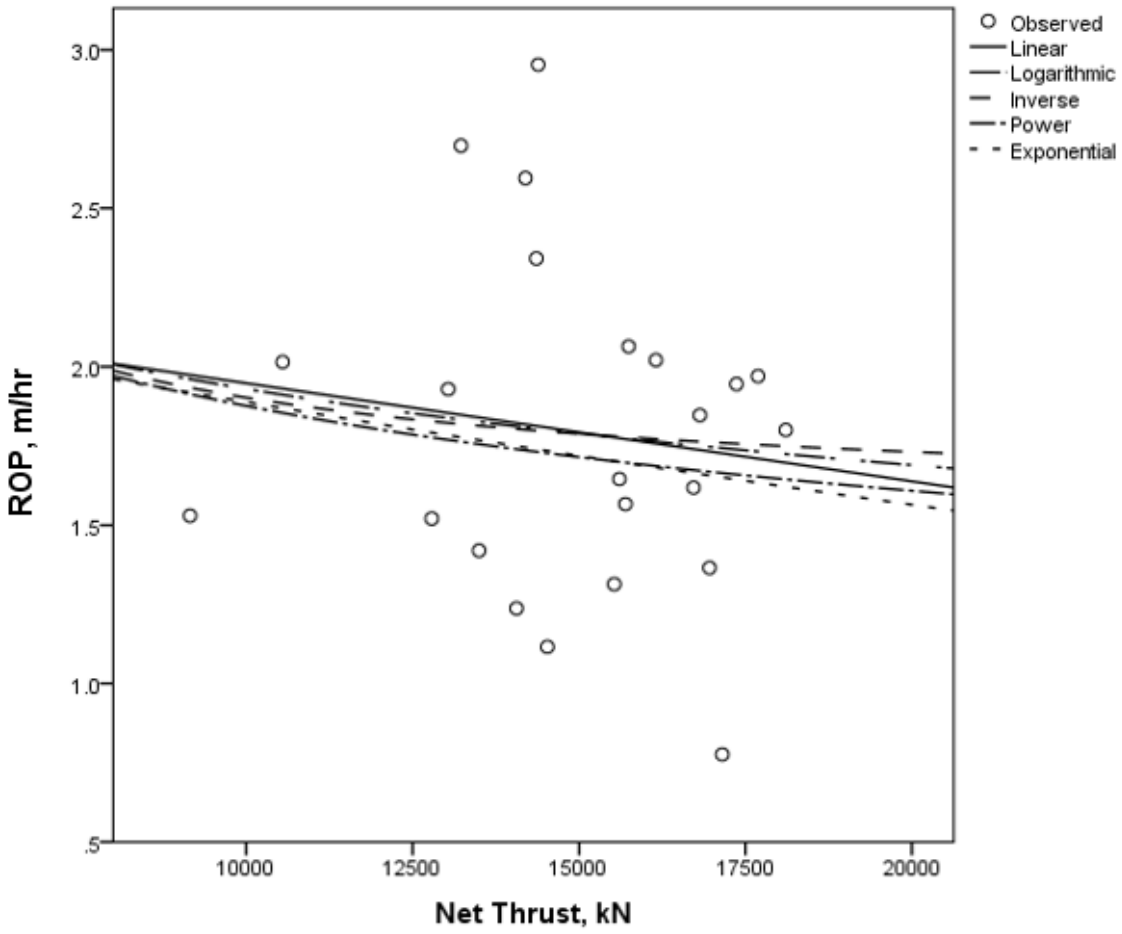

Figure 6. Relationship between ROP and Net Thrust

Table 7. Model summary and parameter estimates for ROP and Cutterhead Torque correlation

	R^2	F	P-value	b_0	b_1
Linear	0.677	43.931	0.000	2.257	0.001
Logarithmic	0.629	35.565	0.000	-8.916	1.520
Inverse	0.569	27.698	0.000	3.135	-1483.865
Power	0.647	38.495	0.000	0.003	0.900
Exponential	0.673	43.227	0.000	0.634	0.001

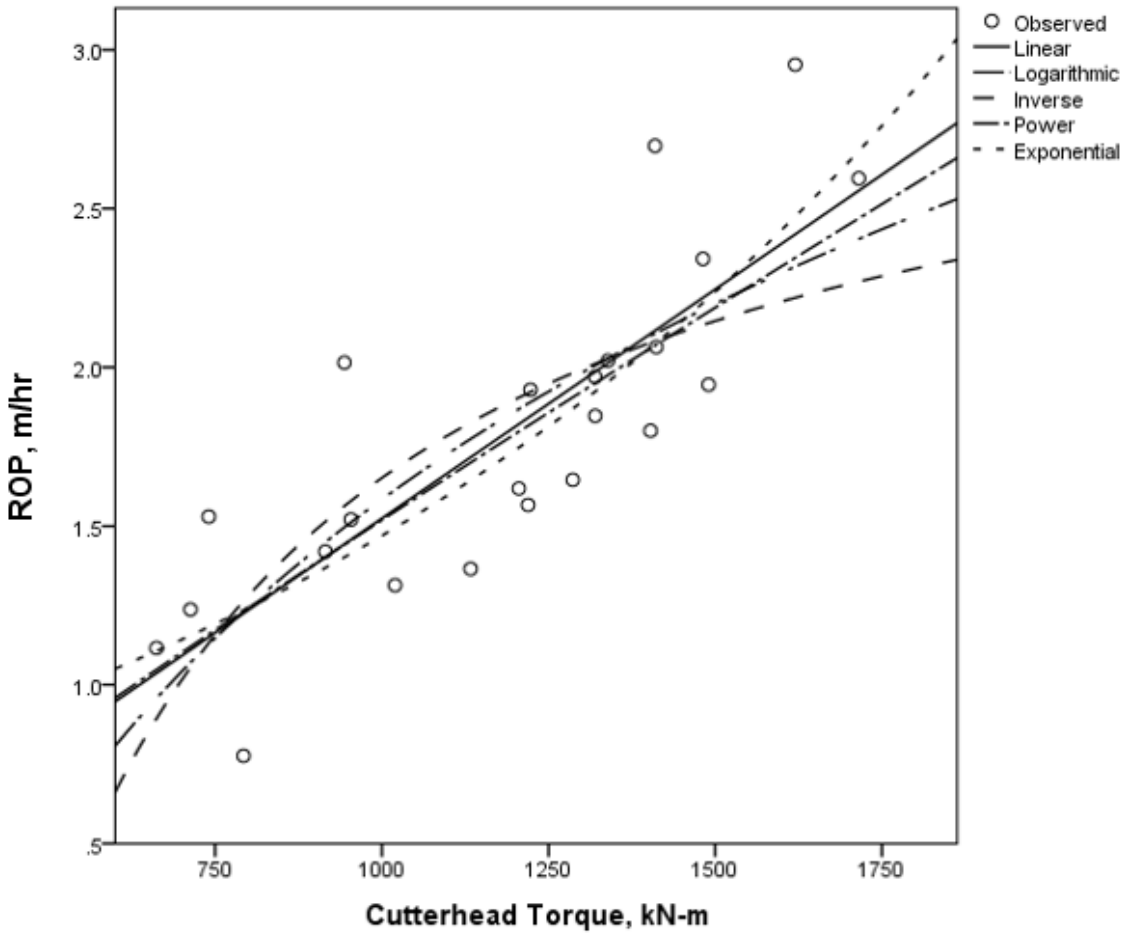

Figure 7. Relationship between ROP and Cutterhead Torque

Blank page